Australian Government
Department of Defence
Defence Science and
Technology Organisation

Evaluation of the C* Model for Addressing Short Fatigue Crack Growth

K.F. Walker and W. Hu

Air Vehicles Division
Defence Science and Technology Organisation

DSTO-TR-2185

ABSTRACT

The C* model has been proposed to account for the breakdown of K-similitude which occurs for short cracks. The model is based on the concept that crack growth rate is dependent not only on the stress intensity factor range, but also on crack length. This report evaluates the C* model using experimental data from the open literature. For comparison, two other models, the El Haddad model and the FASTRAN model, were also evaluated for their capability in dealing with the same problem. The objective of the evaluation was to assess the performance of the C* model compared with the other two models in treating short and long crack growth in a unified manner, and to illustrate their merits and shortcomings. For the cases tested, the C* model was found to be ineffective in resolving the issue of breakdown of similitude for short cracks, and was of less practical use than the other models.

Published by

Air Vehicles Division
DSTO Defence Science and Technology Organisation
506 Lorimer St
Fishermans Bend, Victoria 3207 Australia

Telephone: (03) 9626 7000
Fax: (03) 9626 7999

AR 014-281
October 2008

APPROVED FOR PUBLIC RELEASE

Evaluation of the C* Model for Addressing Short Fatigue Crack Growth

Executive Summary

The accurate modelling of fatigue crack growth in high strength metallic aircraft structures is an essential requirement for the structural integrity management of the aircraft fleets of the Royal Australian Air Force. One of the challenges in the analysis of fatigue crack growth is the apparent anomalous behaviour of short crack growth which cannot be adequately characterised by linear elastic fracture mechanics. In terms of fatigue life, short crack growth plays an important role, as in some structures a significant amount of service life is expended in growing short cracks in the order of microns.

The C* model has been proposed to account for the breakdown of K-similitude which occurs for short cracks. The model is based on the concept that crack growth rate is dependent not only on the stress intensity factor range, but also on crack length. This report evaluates the C* model using experimental data from the open literature. For comparison, two other models, the El Haddad model and the FASTRAN model, were also evaluated for their capability in dealing with the same problem. The objective of the evaluation was to assess the performance of the C* model compared with the other two models in treating short and long crack growth in a unified manner, and to illustrate their merits and shortcomings. For the cases tested, the C* model was found to be ineffective in resolving the issue of breakdown of similitude for short cracks, and was of less practical use than the other models.

Having knowledge of the most accurate and reliable methods of modelling the growth of fatigue cracks in the small crack regime will improve the ability of the RAAF to manage their fleets. Where accurate modelling cannot be done, conservative assumptions need to be made and this leads to higher costs through earlier retirement times and/or more frequent inspections. The work conducted here will assist the Royal Australian Air Force to select the most appropriate modelling techniques and thereby minimise unnecessary conservatism and reduce the cost of ownership and improve aircraft availability.

Authors

K.F. Walker
Air Vehicles Division

Mr Walker graduated in 1983 with a Bachelor of Aeronautical Engineering (with distinction) from RMIT. He then served for eight years with the RAAF, including a posting to the USA where he gained a Master of Science in Aeronautics and Astronautics from Purdue University. He then worked for three years in private industry before joining DSTO AVD in early 1994. His work at DSTO has included fatigue crack growth and damage tolerance analysis studies (mainly related to the F-111 aircraft), evaluation of fatigue monitoring systems, development, design, validation and substantiation of bonded composite repairs, and development of improved fatigue crack growth analysis software. He is currently the lead structures engineer for surveillance aircraft including the P3 Maritime Patrol and the Boeing 737 based AEW&C aircraft.

W. Hu
Air Vehicles Division

Weiping Hu joined DSTO in 1998 as a research scientist. He is currently a senior research scientist leading the development of modelling capabilities for the analysis of structural integrity of aircraft structures.

After obtaining his PhD degree in 1993 at Dublin City Univeristy, Ireland, he held various academic positions at Dublin City University, Monash University and Deakin University. His current research interests include fatigue and fracture of engineering materials and structures, fatigue crack growth in aircraft structures, constitutive models and plasticity, and numerical methods in engineering.

Contents

Nomenclature

a	Crack length, or half length for a symmetric crack.
c	Crack length, or half length for a symmetric crack.
a_0	A material constant which represents a small crack size: $a_0 \approx \frac{1}{\pi}\left(\frac{\Delta K_0}{\beta \Delta \sigma_e}\right)$
C	Crack growth rate coefficient in Paris law.
C^*	Parameter in C* Model
m	Crack growth rate exponent in Paris law.
m^*	Parameter in C* Model
N	Number of cycles.
N_i	Initial Number of Cycles
N_f	Fatigue life; the number of cycles to fatigue failure.
K	Stress intensity factor.
ΔK	Stress intensity factor range.
ΔK_0	Long crack threshold. It is considered to be a material constant, and in particular, independent of crack length.
ΔK_{eff}	Effective stress intensity range.
R	Stress ratio of a load cycle, $R_S = S_{\min} / S_{\max}$.
S	Applied remote stress.
ΔS_{eff}	Effective stress range, $\Delta S_{eff} = S_{\max} - S_{open}$
$S_{\max}$	The maximum stress in a load cycle.
S_o	Crack opening stress.
ΔS	Applied stress range. $\Delta S = S_{\max} - S_{\min}$.
β	Geometry correction factor, which is a function of crack size and component geometry.
ρ	Monotonic plastic zone size.
$\Delta \sigma_e$	Endurance limit.
ω	Dugdale cyclic plastic zone size.
ϕ	Constant in C* model

1. Introduction

The assessment of structural fatigue life and crack growth is an essential element in the management of structural integrity of military aircraft fleets. For structures that were designed according to the safe life methodology, the total life may be modelled as a combination of crack initiation life and (long) crack growth life, or alternatively as simply crack growth life encompassing short and long cracks. With the advancement in experimental and computational techniques, there is a trend to expand crack growth analysis into cracks of the length scale traditionally treated as crack initiation. This is the so-called "short" or "small" crack regime in which the stress intensity factor (SIF) range (ΔK) similitude is known to break down [1]. Typically, short cracks grow faster than long cracks when subjected to the same ΔK (for constant amplitude loading), and they may continue to grow below the long crack threshold as illustrated in Figure 1. Short cracks may initially grow at a decreasing rate, and then accelerate to merge with the growth rate of long cracks, or they may stop growing altogether, as illustrated by the dashed lines in Figure 1. As shown here, a fourth regime may be identified in addition to the traditional three regions of SIF range. In addition to the threshold regime, stable growth regime and the fracture regime for long cracks, there is a short crack regime. Short cracks exhibit different behaviour to long cracks when subjected to the same ΔK . For example, at point A, the long crack growth rate is below the short crack growth rate, and at point B, the long crack ceases to grow but the short crack continues to grow. These phenomena are collectively referred to as short crack effects, or short crack anomalies, and cannot be readily represented by growth rate laws such as the Paris law [2]. From the viewpoint of linear elastic fracture mechanics (LEFM), short crack effects demonstrate a breakdown of the similitude principle, *i.e.*, ΔK is no longer a unique correlating parameter for crack growth rate. This "anomalous" growth behaviour of short cracks was first observed by Pearson [3], and has been studied extensively by numerous researchers (for example [1, 4-8]). These phenomena have practical engineering significance because the predictions of short crack growth based on LEFM usually lead to non-conservative growth rate, inspection intervals or possibly critical crack size [9] if they are not modelled properly.

The technical relevance of short crack growth is manifested in the fact that the major part of the fatigue life of components managed according to the concept of durability and damage tolerance is generally spent on growing micro and short cracks. Consequently, a significant amount of research work has been conducted to understand and model short crack growth. In a classical paper on short crack growth by Suresh and Ritchie [1], a comprehensive review was given to the then state-of-the-art in the research of short crack effects, including different techniques used for measuring short cracks, the generation of short cracks, the measurement of short crack thresholds and crack closure, and the breakdown of similitude for three types of short cracks. From the viewpoint of engineering application, a critical issue for short crack modelling is the use of long crack growth rate data to predict short crack growth behaviour. This is extremely desirable because short crack growth data are difficult and expensive to acquire. Indeed, using long crack data to predict short crack growth has been the central issue for short crack modelling.

Recently, Jones *et al.* proposed a crack growth model referred to as the C^* model, after the principal parameter of the model [5-7]. The model aims to deal with the breakdown of similitude in Region I and the lower end of Region II (see Figure 1), by introducing an explicit crack length term into the rate equation. In this report, we evaluate the C^* model, using experimental crack growth data obtained from the open literature. Specifically, the report focuses on examining:

a. The extent to which the model can address short and long cracks in a unified manner;
b. Whether the model is able to deal with short and long cracks in Region I (see Figure 1);
c. Whether the model works for the whole of Regions I and II.

For comparison, two existing models, the El Haddad model [10] and the FASTRAN [11] model are also examined.

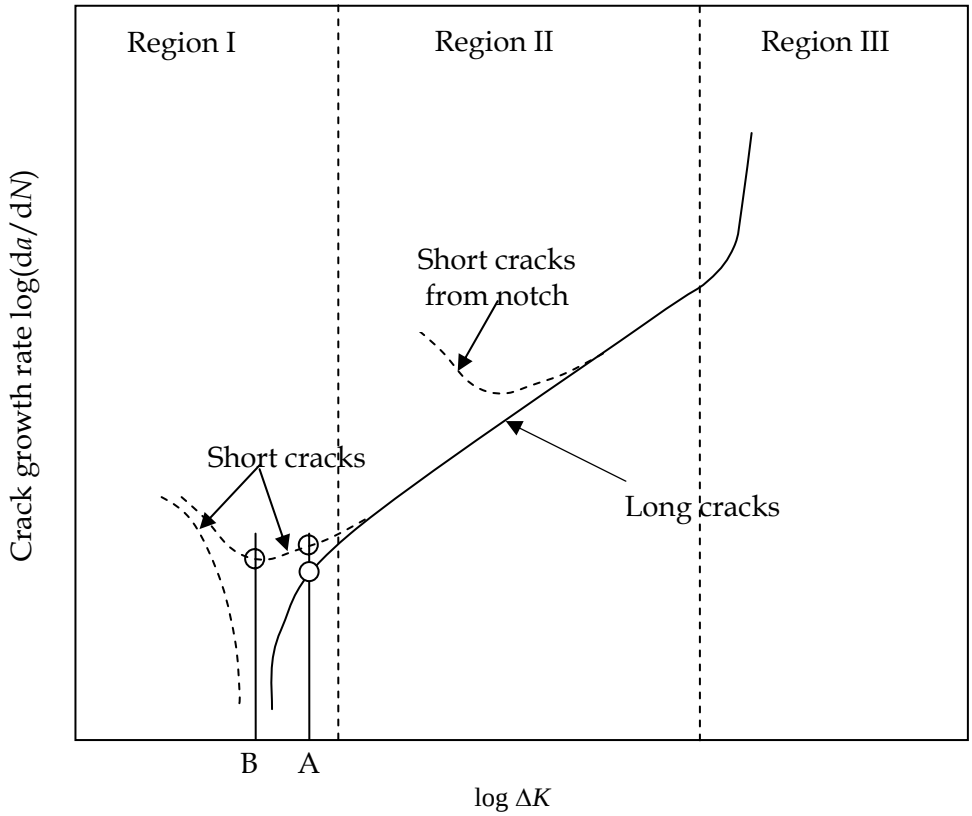

Figure 1: Illustration of typical long and short crack growth rates as a function of stress intensity factor range, under constant amplitude loading. Short cracks grow at below the threshold value for long cracks. They may either develop into long cracks or arrest. Short cracks emanating from notches usually develop into long cracks (adapted from [1]).

2. Analytical Models

Over the last few decades, numerous models have been proposed to account for short crack effects, with varying degrees of success. A comprehensive review of short crack research is beyond the scope of this report, but several good review papers may be consulted for this, e.g. [1, 9, 12]. In this section, we summarise the C^* model proposed by Jones *et al.* [5-7], and two reference models; the El Haddad model [10], and the FASTRAN model [11], to define the scope for the evaluation.

2.1 C* Model

Based on the experimental observation that for a wide class of engineering problems the crack growth appears to be exponential, Jones *et al.* [5-7] proposed that in the low to mid range ΔK region (Region I), the crack growth rate may be expressed as;

$$\frac{da}{dN} = C^* a^{1-m^*/2} \Delta K_{\text{eff}}^{m^*} \tag{1}$$

where C^* and m^* are constants, a is the crack length, and ΔK_{eff} is the effective applied stress intensity range. It was suggested [5-7] that by making the crack growth rate explicitly depend on the crack length as well as the stress intensity range, the "breakdown of similitude" in Region I may be removed, however this point was not clearly illustrated in [5, 6]. It was not clear, for example, whether the "breakdown of similitude" refers to the short crack effect, or the threshold behaviour of long cracks, as represented in Figure 1 by the dashed and solid lines, respectively. From the plots presented in [5, 6], it appears that the breakdown of similitude refers to the threshold behaviour of long cracks, but no evidence was given to demonstrate that two long cracks of different sizes, when subjected to the same SIF range, will grow at different rates. These observations notwithstanding, it is worthwhile to investigate the applicability of the model to the short crack regime, the threshold regime and the Paris regime[1].

By examining the selected experimental data, it was suggested in [5, 6] that $m^* = 3$ in Eqn (1), *i.e.*,

$$\frac{da}{dN} = C^* \Delta K^3 / \sqrt{a} \tag{2}$$

Thus, the fatigue crack growth rate is described by a single parameter, the coefficient of crack growth rate C^*.

A general form of Eqn (1) reads,

$$\frac{da}{dN} = C^* a^{\phi} \Delta K^{m^*} \tag{3}$$

[1] The Paris regime is Region II (see Figure 1). In this regime it is generally accepted that similitude holds and LEFM is valid.

which allows the exponents ϕ and m^* to vary independently. Eqn (1) is recovered by assuming $\phi = 1 - m^*/2$, and Eqn (2) is recovered by further setting $m^* = 3$.

It should be noted that Eqn (1) is in effect the Frost-Dugdale model for log-linear growth [13] when the geometry factor (β) is constant, as shown here:

$$\begin{aligned}
&\frac{\mathrm{d}a}{\mathrm{d}N} = C^* a^{(1-m^*/2)} \left(\Delta K_{\text{eff}}\right)^{m^*} \\
&= C^* a^{(1-m^*/2)} \left(\beta \Delta S \sqrt{\pi a}\right)^{m^m} \\
&= C^* a^{(1-m^*/2)} a^{m^m/2} \left(\beta \Delta S \sqrt{\pi}\right)^{m^*} \\
&= C^* \left(\beta \Delta S \sqrt{\pi}\right)^{m^*} a \\
&= \lambda a
\end{aligned} \tag{4}$$

The intention of the Eqn. 1 representation of the Frost-Dugdale model is so that existing and widely available experimental data (a , $\mathrm{d}a/\mathrm{d}n$, ΔK) can be investigated. The attractiveness of the Eqn. 2 version of the model is that there is only one parameter (C^*) to determine. Note that the value of C^* will be unique for each combination of material, stress level and spectrum, and therefore needs to be derived from experimental data. Both Equations 2 and 3 (for m^*=3) are evaluated in this report.

2.2 El Haddad Model

Within the framework of LEFM, the short crack effects may be modelled by adopting an artificial crack length of $a + a_0$ for stress intensity range calculation [10], where a is the physical crack length and a_0 a material parameter. Thus,

$$\Delta K_{\text{eff}} = \beta(a) \Delta S \sqrt{\pi (a + a_0)} \tag{5}$$

which results in a significant increase in the effective stress intensity range when the crack length is comparable to a_0, but this magnifying effect diminishes when the physical crack is much longer than a_0. It thus approximates the observed short crack effects. In this model, the material-dependent parameter a_0 was estimated from the limiting conditions of crack length when the nominal stress range ΔS approaches the fatigue limit $\Delta\sigma_{\text{e}}$ and when ΔK approaches the long crack threshold intensity range ΔK_0 at $R = 0$. Hence,

$$a_0 = \frac{1}{\pi} \left(\frac{\Delta K_0}{\beta \Delta \sigma_e} \right)^2 \tag{6}$$

2.3 FASTRAN Model

In the FASTRAN model [11], a similar concept to that of the El Haddad model was used. Instead of adding a constant parameter a_0 to the physical crack size, a variable ω is added.

Here, ω is dependent on the crack tip plastic zone size ρ caused by the maximum stress. The effective stress intensity factor range is thus calculated as

$$\Delta K_{\text{eff}} = \beta \Delta S_{eff} \sqrt{\pi(a+\omega)} \tag{7}$$

where $\Delta S_{eff} = S_{\max} - S_o$ is the effective stress range, and $S_{\max}$ and S_o are the maximum stress in the current load cycle and the crack opening stress, respectively. In FASTRAN3.8[2], several options were implemented for the calculation of ω, and one of them is

$$\omega = 0.05\rho(1-R)^2 . \tag{8}$$

Of course, this modification to the stress intensity range in FASTRAN is in addition to the crack closure model, which itself also helps to model the short crack effects, as discussed later.

A variation on the FASTRAN model was also examined. It is a combination of the FASTRAN and El Haddad models. Instead of adding ω to the crack length, the El Haddad a_0 is added. So, the stress intensity range is calculated in CGAP as follows:

$$\Delta K_{\text{eff}} = \beta \Delta S_{eff} \sqrt{\pi(a+a_0)} , \tag{9}$$

in which the FASTRAN crack closure model is used to calculate the effective stress range.

2.4 Model Evaluation Approach and Scope

The approach and scope for model evaluation presented in this report are as follows. The performance of the C^* model was evaluated using experimental data obtained from the open literature. Since there is only one parameter for the C^* model, its performance is principally decided by this parameter, C^*. It is therefore important to accurately determine the parameter from the given experimental data, and to explore whether a consistent single parameter can account for long and short crack data. It is also important to determine the extent of applicability of the model in Regions I and/or II. Where appropriate, the reference models were used to generate crack growth data for comparison. It is important to highlight that the two reference models use the parameters determined from the long crack data only.

The C^* and the El Haddad models were implemented in a purpose-built FORTRAN program. The El Haddad model and the FASTRAN model were integrated into CGAP [14].

The short crack growth data for the current evaluation were selected from [8] for two high strength aluminium alloys: LC9cs and 7075-T6. LC9cs is a Chinese alloy similar to 7075-T6 except it is clad. The long crack growth rate data were also obtained from [8]. A brief description of the experimental data is given in Section 3.

[2] FASTRAN3.8 is an update of FASTRAN II

3. Experimental Data

The experimental data used for the current evaluation are detailed below. These data are used for both model identification and model verification.

3.1 Geometry and Loading

The short crack experimental data available in [8] included those for constant amplitude and spectrum loading tests on single edge notched tension (SENT) specimens of the LC9cs and 7075-T6 aluminium alloy. The SENT specimens were 2 mm thick and 50 mm wide, with a semi-circular edge notch of radius 3.2 mm on one side. The specimen design is shown in Figure 2, and the crack geometry is detailed in Figure 3.

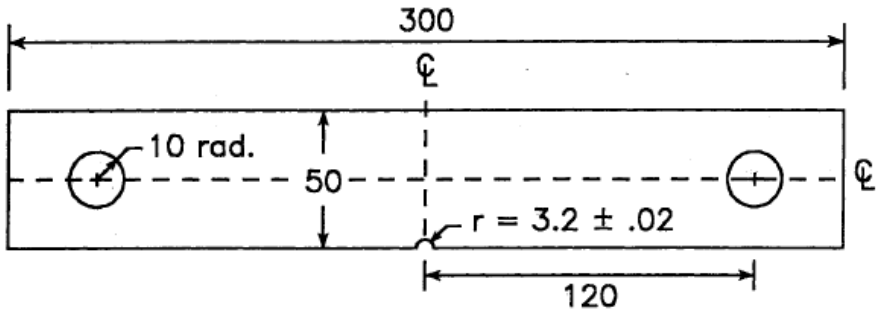

Figure 2: Single Edge Notch Tension Specimen [8], dimensions in mm

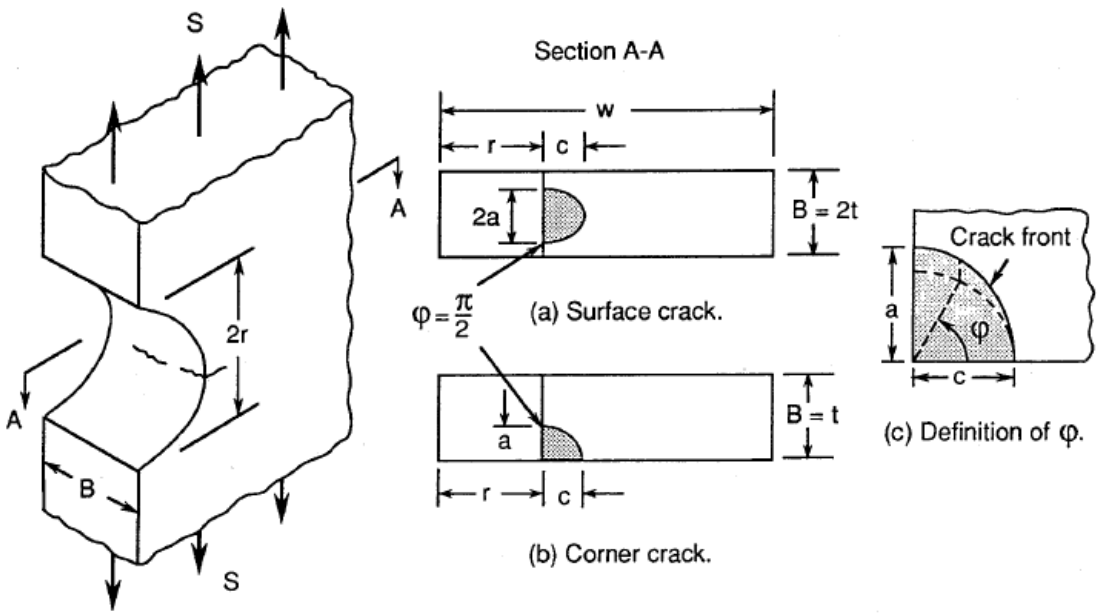

Figure 3: Definitions for crack characterisation for SENT specimens. Adapted from [8]

For the constant amplitude loading, the specimens were tested under three different stress ratios and two stress levels for each stress ratio. For the LC9cs material, the stress levels in terms of S_{max} were 70 and 90 MPa at $R=-1$, 100 and 115 MPa at $R=0$, and 165 and 185 MPa at $R=0.5$. For the 7075-T6 material, the stress levels in terms of S_{max} were 80 and 95 MPa at $R=-1$, 120 and 140 MPa at $R=0$, and 195 and 220 MPa at $R=0.5$.

It is important to define the parameters which are used in this report to quantify the cracking. These are shown in Figure 3 which was adapted from [8].

3.2 Crack Growth Properties

3.2.1 LC9cs Alloy Short and Long Crack Growth Data and Geometry Factor

The most useful way to evaluate the performance of the C^* model compared with the other models is to compare analytical versus experimental results in terms of crack size plotted against the number of cycles of applied loading. In the case of the LC9cs data in [8], the only case for which short crack data was explicitly available in that form was for constant amplitude loading at $R=-1$ and $S_{max}=90$ MPa. This case, as expected, produced the most significant short crack effects, and hence it has been chosen for the main evaluation. For comparison, the cases of $R=0, S_{max}=115$ MPa and $R=0.5, S_{max}=185$ MPa were also analysed using the El Haddad model. The experimental crack growth curves for $R=-1$ are re-produced in Figure 4, in which the crack length is the length along the bore of the notch for a semi-circular corner crack, with an aspect ratio of approximately $a/c=1$ (see Figure 3 for definitions). This was the typical form of cracking for this case, and most cracks initiated as corner cracks at the interface with the clad layer.

The long crack growth rate data for LC9cs is shown in Figure 5. The straight line represents the Paris law with $C=1.9221E-11$ and $m=3.0384$. These parameters are subsequently used for the evaluation of the El Haddad model while the da/dN versus ΔK_{eff} data as per [8] is used for the FASTRAN model evaluation. The geometry factor (β) solution for a single, semi-circular ($a/c=1$) corner crack was extracted from CGAP, which is essentially an implementation based on the solution given in [8]. The geometry factor as a function of crack length is plotted in Figure 6. This geometry factor solution was used for the evaluation of the El Haddad and C^* models for the LC9cs alloy case. In the case of FASTRAN/CGAP, the internal solution which evaluates the crack growth independently in the thickness and width direction was used. The analysis resulted in the crack retaining a shape very close to semi-circular throughout its life in any case, so the solution as per Figure 6 is very close to that used for the FASTRAN/CGAP analysis.

The initial crack size used for all the models is 77 μm, as per [8]. From the viewpoint of engineering application, the initial crack size plays a significant role in the crack growth life analysis, but a detailed discussion on this is beyond the scope of the current report. The current initial crack size is based on experimental observation as per [8].

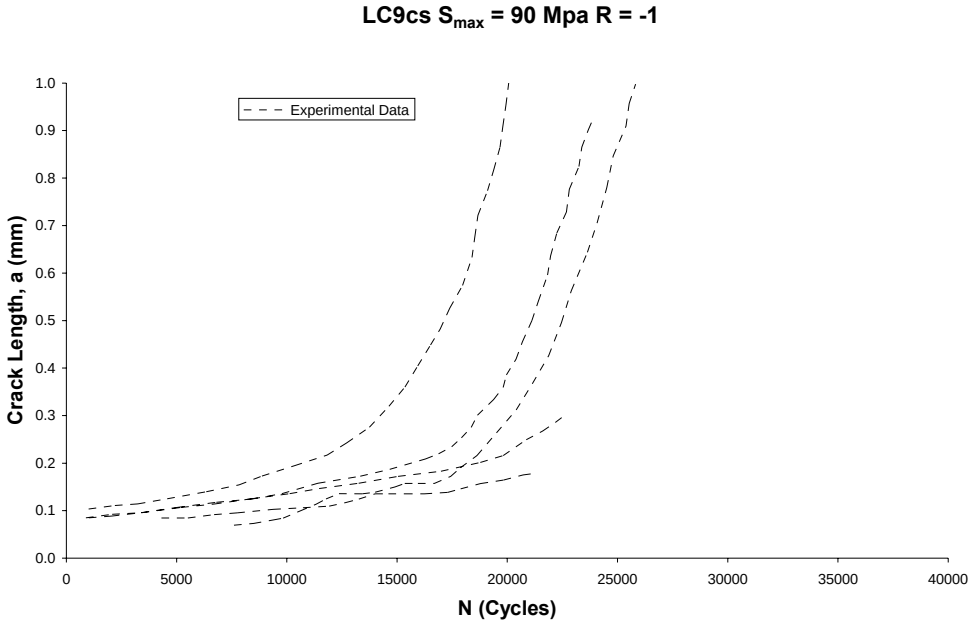

Figure 4: Experimental short crack growth for SENT specimen, constant amplitude loading, $R = -1$ and $S_{\max} = 90$ MPa, LC9cs aluminium alloy. Reproduced from [8]

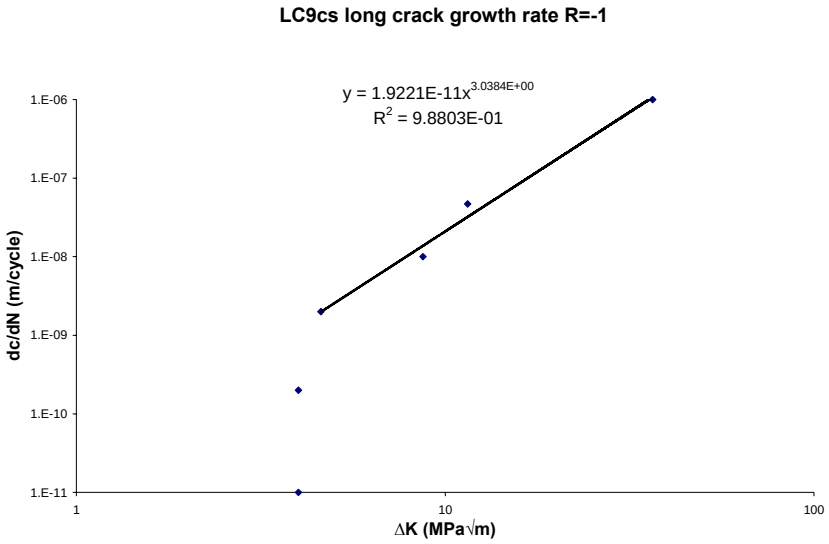

Figure 5: Long crack growth rate data LC9cs alloy $R = -1$, from [8]. Note that the power curve fit (Paris type equation) ignores the data near the threshold region, i.e. the two data points below 1e-9 m/cycle.

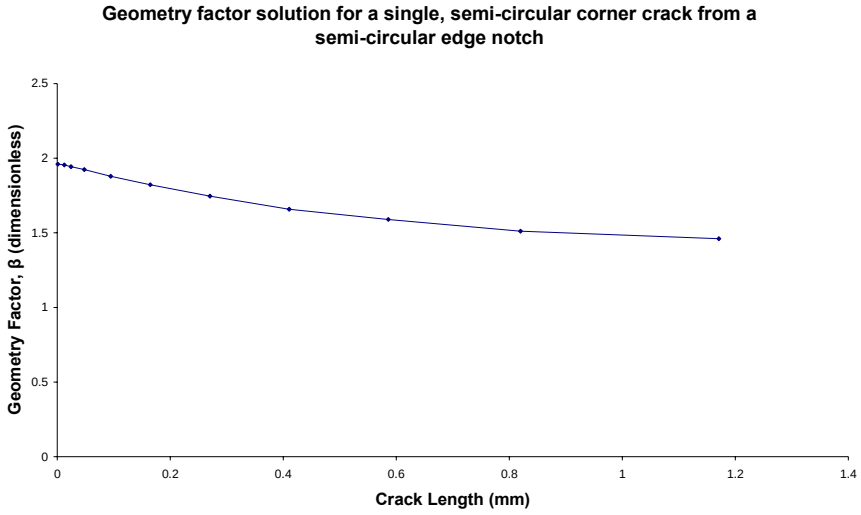

Figure 6: Geometry factor solution for a single, semi-circular corner crack emanating from an edge notch as per Figure 2, extracted from FASTRAN/CGAP. Solution is for the "a" direction as per the definitions in Figure 3.

3.2.2 7075-T6 Alloy Short and Long Crack Growth Data and Geometry Factor

Similar to the case for LC9cs alloy, the only case where crack length against cycle short crack data were presented in [8] for 7075-T6 was for constant amplitude loading at $R=-1$ and $S_{\max}=95$ MPa. Again, this case produced the most significant short crack effects, and hence it has been chosen for the evaluation. The experimental crack growth curves for $R=-1$ are re-produced in Figure 7. The crack length in Figure 7 is the tip to tip length (L=2a) along the bore of the notch for mid-thickness, semi-circular surface crack, with an aspect ratio of approximately $a/c=1$. The cracks observed in the 7075-T6 specimens were typically of that form. As reported in [8], it was discovered that the replica technique affected the crack growth rate. This is discussed as appropriate in this report when assessing the results and comparing analysis with test data.

Similar to the LC9cs alloy, the long crack growth rate data are plotted in Figure 8 and fitted to the Paris law, to give $C=1.0887E-11$ and $m=3.1697$. These parameters were used for the evaluation of the El Haddad model while the da/dN versus ΔK_{eff} data as per [8] were used for the FASTRAN model evaluation. The geometry factor (β) solution for a single mid-thickness, semi-circular surface crack, with an aspect ratio of $a/c=1$ was extracted from CGAP and is plotted against a in Figure 9. This geometry factor solution was used for the evaluation of the El Haddad and C^* models for the 7075-T6 case. A similar approach to that for LC9cs was adopted for the FASTRAN/CGAP analyses.

The initial crack size used for all the models is $a=3$ μm ($L=2a=6$ μm) and $c=9$ μm, as per [8]. Although this initial crack shape is not semi-circular (a/c=1), the cracks almost immediately become semi-circular in shape. Further details are provided in [8].

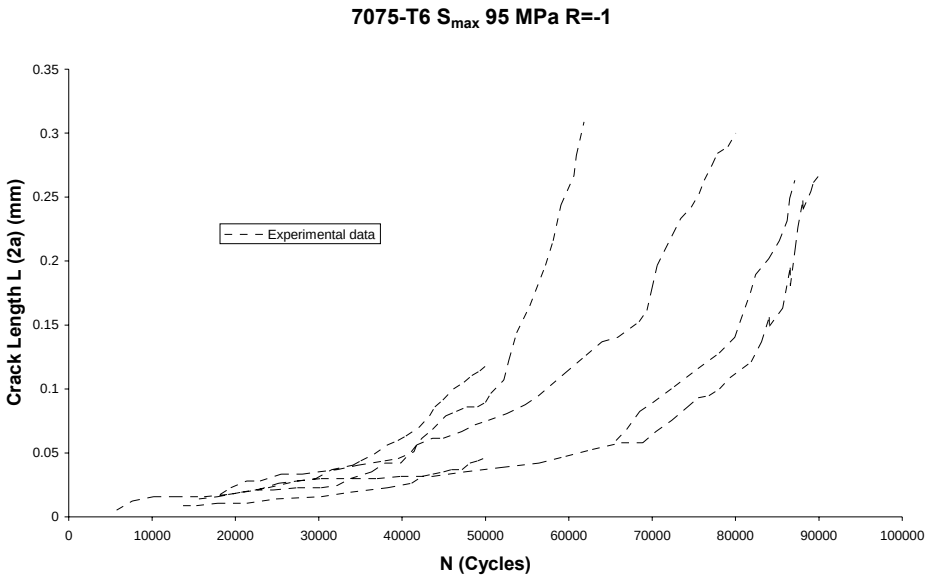

Figure 7: Experimental short crack growth for SENT specimen, constant amplitude loading, $R = -1$ *and* $S_{\max} = 95$ *MPa, 7075-T6 aluminium alloy. Reproduced from [8]*

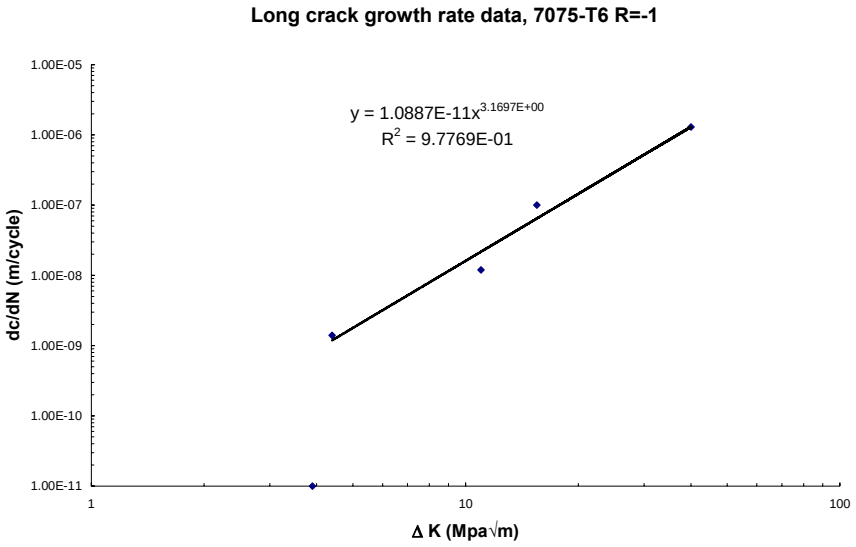

Figure 8: Long crack growth rate data 7075-T6 alloy $R = -1$*, from [8]*

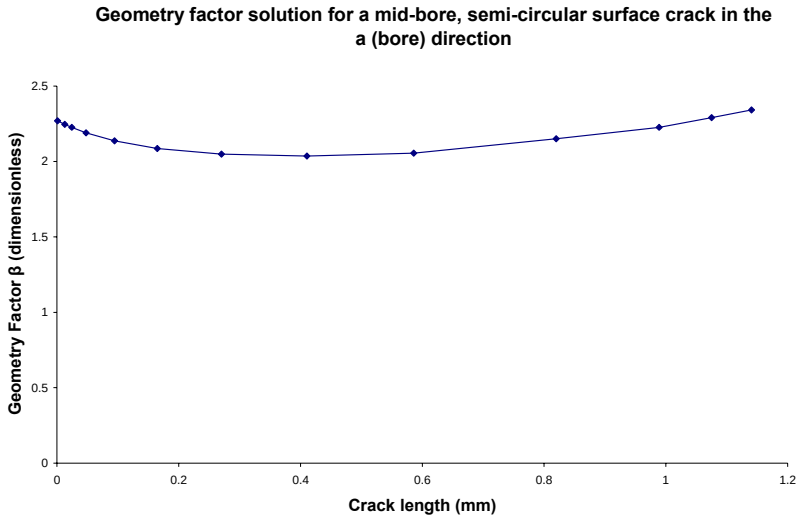

Figure 9: Geometry factor solution for a single mid-bore, semi-circular surface crack emanating from an edge notch as per Figure 2, extracted from FASTRAN/CGAP. Solution is for the "a" direction as per Figure 3.

4. Preliminary Evaluation: Short Cracks

In this section, predictive capability of the C^* model was evaluated using short crack data to predict short crack growth. In contrast, both reference models were evaluated using long crack data to predict short crack growth, which is a more desirable capability. Further examination of the models is presented in Section 5. In this preliminary evaluation of the C^* model data from both Regions I and II are included. It is important to note that the developers of the C^* model have stated that for constant amplitude loading the method is proposed for Region I and the lower portion of Region II only (see Figure 1 from [6]). This aspect is considered in detail later in Section 5.

4.1 C* Model – Using Short Crack Data to Predict Short Crack Growth

As discussed in Section 2.1, the C^* model attempts to deal with the breakdown in similitude by introducing an explicit crack length dependency, in addition to the stress intensity dependency, into the crack growth rate equation, as represented by Eqn. 2. The only model parameter to be determined is C^*, but to determine this parameter, the crack length a corresponding to, and in addition to, the normally-reported test data $(da/dN, \Delta K)$ is required. Where this information was not directly available from [8], it was recovered by solving the following nonlinear equation[3], if the applied stress range is known,

$$\Delta K = \Delta S \beta(a) \sqrt{\pi a} \tag{11}$$

Once the triplets $(a, da/dN, \Delta K)$ are calculated, Eqn. 2 may be plotted to determine the parameter C^*. On a linear-linear scale of da/dN versus $\Delta K^3/\sqrt{a}$, C^* is the slope of the straight line that best fits the experimental data. To calculate crack growth using the C^* model, Eqn. 2 may be reformatted to give

$$\frac{da}{dN} = C^* \left(\Delta S \sqrt{\pi}\right)^3 \beta^3(a) a\,, \tag{12}$$

which can be integrated with respect to crack length[4].

4.1.1 LC9cs Alloy

The short crack growth rate data, $\mathrm{d}a/\mathrm{d}N$ versus $\Delta K^3/\sqrt{a}$, are plotted in Figure 10 according to Eqn. 2. A conditional linear regression was then performed by fixing the y-axis intersect to zero. This gives a C^* model parameter of $C^* = 7.8836 \times 10^{-13}$. By using the β solution from FASTRAN/CGAP [14, 15] for a semi-circular corner crack that maintains a semi-circular shape throughout its life, the crack growth life was obtained by integrating Eqn. 12. The result for $R = -1$ and $\sigma_{\max} = 90$ MPa is plotted in Figure 11.

[3] This was achieved using a small Fortran program called "Calc_a" detailed in Appendix A

[4] This was achieved using a small Fortran program called "CA_Integration" detailed in Appendix B

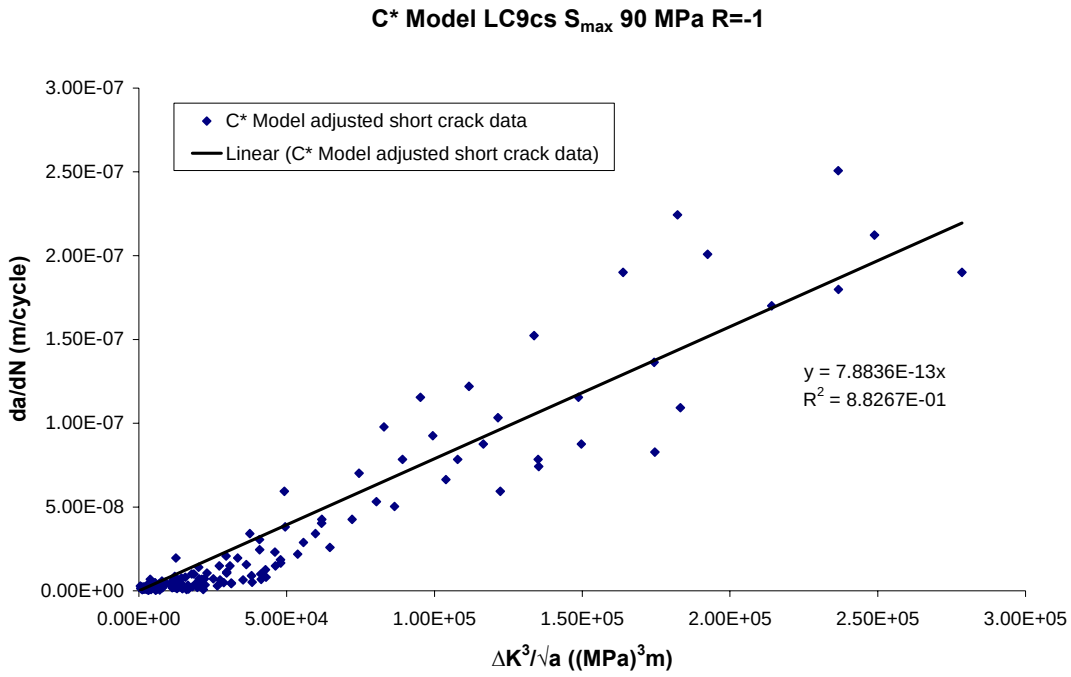

Figure 10: Short crack growth rate data LC9cs alloy $R = -1$, from [8], replotted according Eqn. 2

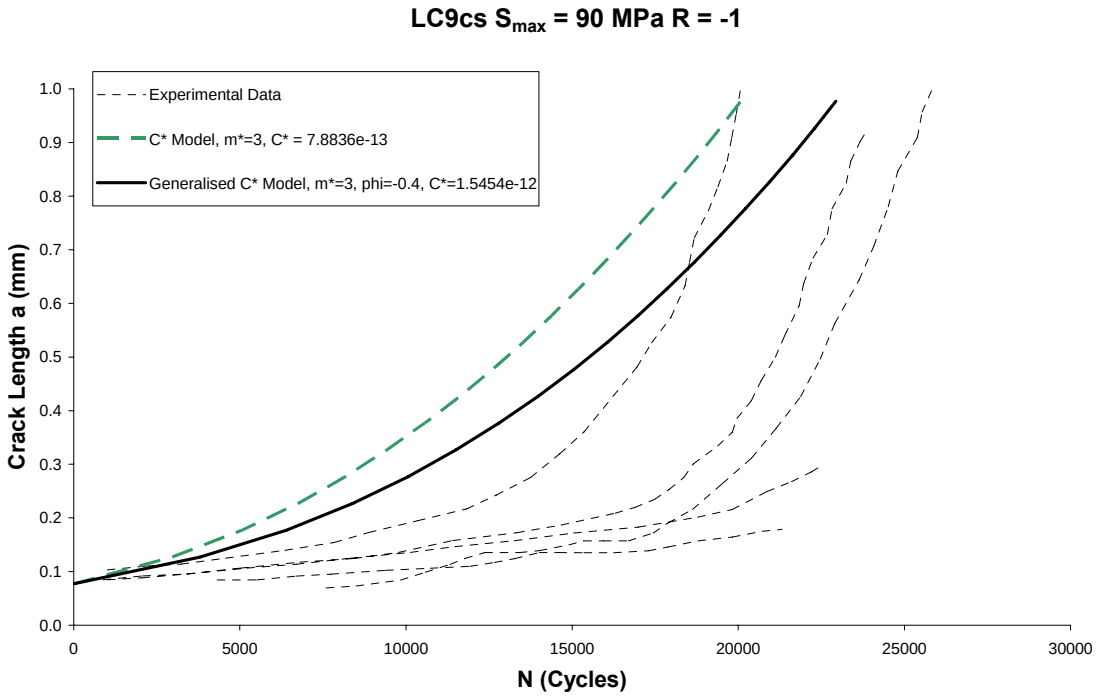

Figure 11: Crack growth curve showing C predictions for LC9cs alloy S_{max} = 90 MPa R=-1*

An attempt was also made to evaluate the generalised model, Eqn. 3, to see the effect of the exponent to a on the crack growth behaviour. Trial–and-error was used to determined the best value for ϕ, and a value of -0.4 was obtained, as shown in Figure 12.

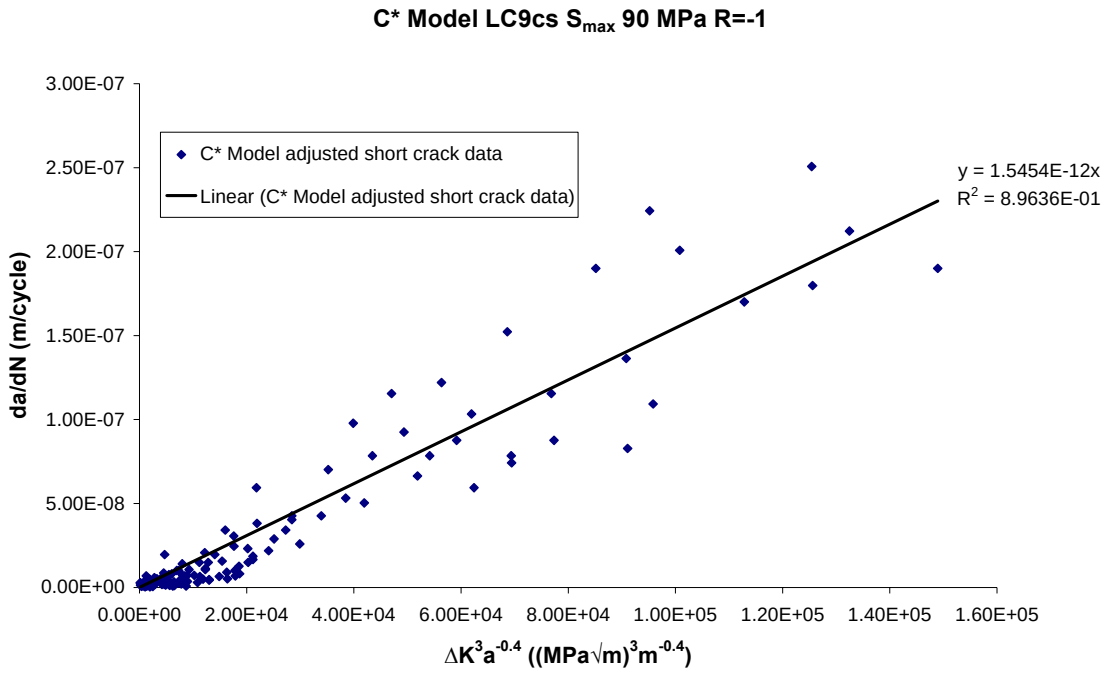

Figure 12 Short crack growth rate data LC9cs alloy, from [8], replotted according to Eqn. 3, with $\phi = -0.4$.

The plot shows a slight improvement in terms of the regression parameter R^2. Note that $\phi = -0.5$ corresponds to the specific case represented by Eqn. 2. The crack growth rate equation corresponding to Eqn. 3 becomes

$$\frac{da}{dN} = C^* \left(\Delta S \sqrt{\pi}\right)^{m^*} \beta(a)^{m^*} a^{\phi + m^*/2} \tag{13}$$

The crack growth results are also plotted in Figure 11.

As can be seen in Figure 11, both Eqn. 2 and 3 produced a reasonable representation of the experimental crack growth in terms of the total life. However, the shape of the crack growth curve was poor, due to the over-estimation of the growth rate when the crack is very short, as can be seen in Figure 10 and Figure 12. It should be noted that since there is only one parameter in the C^* model, i.e. the parameter that defines exponential growth, the shape of the curve is essentially fixed. It is also important to highlight that there has not been a true "prediction" here at all, because the same short crack data is used for both determining the C^* parameter (Figure 10 and Figure 12), and for comparison with the analysis (Figure 11).

To further highlight the difficulty of identifying a single, constant value of C^*, the data represented in Figure 10 were re-plotted after first calculating a value of C^* for each data

point (using Eqn. 2). The result is shown in Figure 13. The C^* value determined earlier is also shown on the plot. It is clear that significant scatter in the C^* parameter is evident, particularly at the shorter crack lengths where a lower value would be more appropriate.

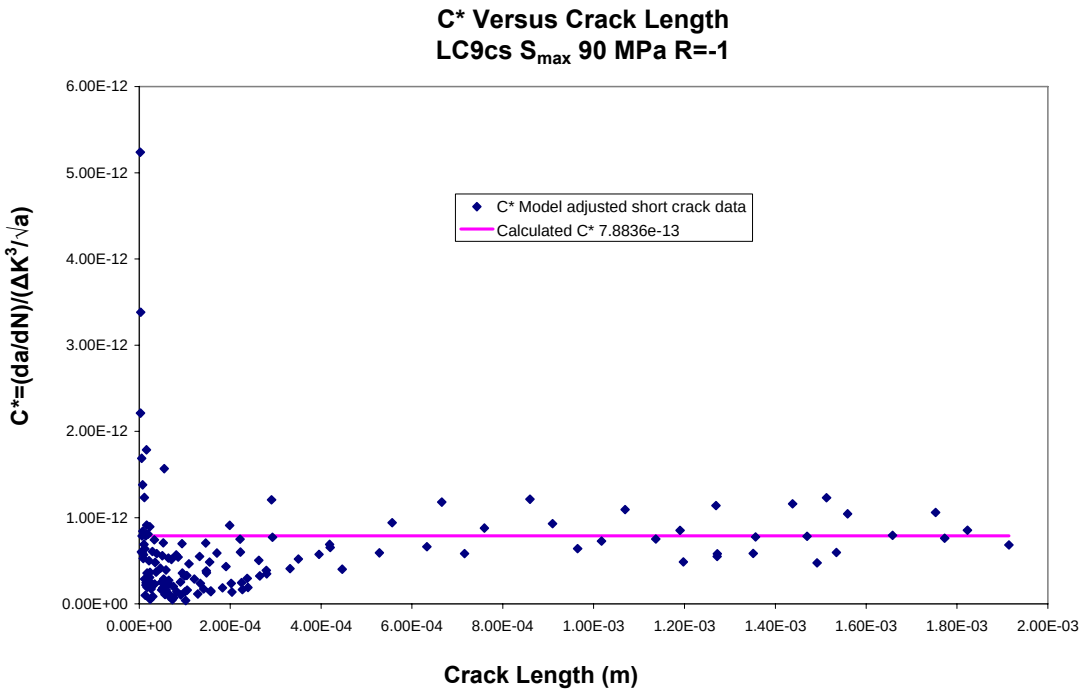

Figure 13: C as a function of crack length for the LC9cs R=-1 case*

4.1.2 7075-T6 Alloy

A similar process to that used for the LC9cs data was applied to the 7075-T6 data. In this case, only Eqn. 2 was used because Eqn. 3 had already been evaluated for LC9cs . Figure 14 plots the experimental data according to Eqn. 2, and straight line defining C^* (green dashed), using all the short crack data. The crack growth curve, predicted by the C^* model is represented by the green dashed curve in Figure 15.

It is clear from Figure 14 that the slope of the green dashed line was significantly affected by the few points with higher growth rate, which corresponds to larger crack length. Since the experimental data only included cracks up to $L = 2a = 0.3$ mm, a case was also analysed in which the curve fit for C^* was restricted to data at and below that crack size. This resulted in a lower value of C^* (see the purple solid line in Figure 14) and consequently a longer life (see the purple line in Figure 15). It is clear that the restriction did result in an improvement in the analysis.

In this case, the issue of the effect of the replica technique on the crack growth measurement[5] is not relevant because the data used for the analysis is the same data for the results to be compared against. Thus far, the C^* model has been used to represent the original crack

[5] This was an issue for the 7075-T6 material as explained in [8].

growth data. In that sense, the model, at least as it has been applied here, does not provide a prediction at all. It is clear from Figure 15 that when the data set used to determine the value for C^* is appropriately restricted, a better result is obtained.

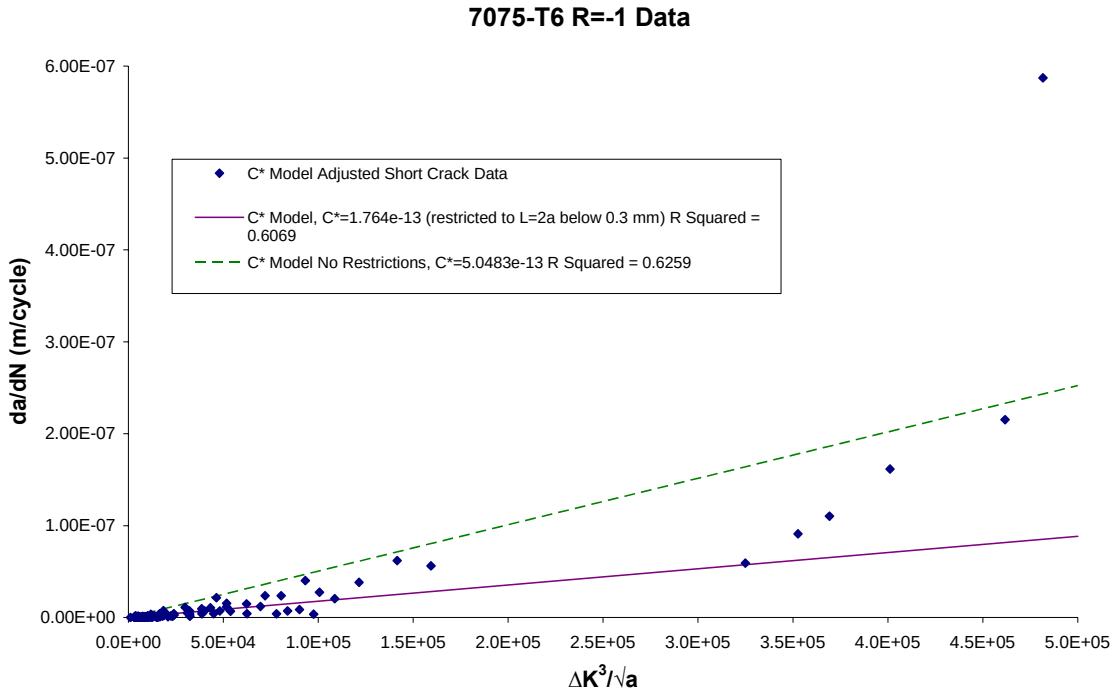

Figure 14: Short crack growth rate data 7075-T6 alloy R=-1, from [8], replotted according to Eqn. 2

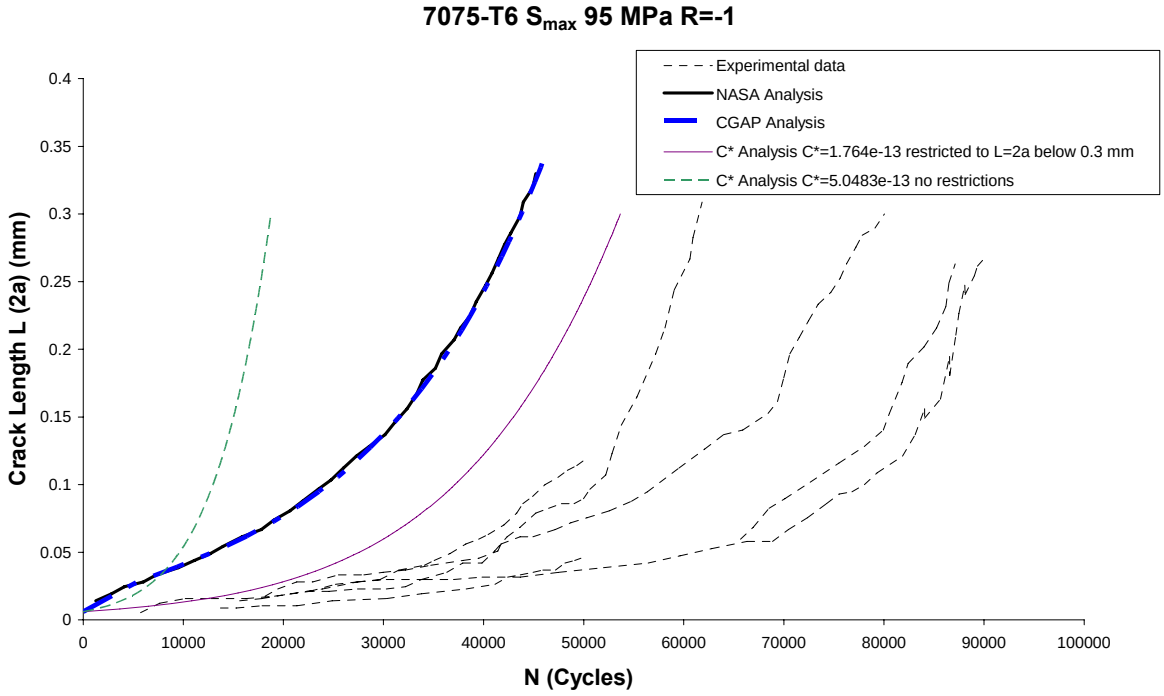

Figure 15: Crack growth curve showing short crack based C predictions for 7075-T6 alloy*

4.2 El Haddad Model – Using Long Crack Data to Predict Short Crack Growth

For the El Haddad model described in Section 2.2, the required model parameters are C and m. These were determined using long crack data, as shown in Figure 5 and Figure 8 for LC9cs and 7075 alloys, respectively. The Paris equation was then integrated to obtain the crack growth curve. It was necessary to compare the crack growth curves as there is no direct comparison between the crack growth rate for the C^* and El Haddad models.

4.2.1 LC9cs Alloy

In this case, the values for ΔK_0 and $\Delta\sigma_e$ were available from [8] and they are 2.4 MPa√m and 100 MPa, respectively, which gives $a_0 = 0.05$ mm according to Eqn. 6. The concept of the El Haddad model was to increase the stress intensity range for short cracks, so that for a crack size comparable to a_0, the crack growth rate is higher than the value obtained from long crack growth rate data.

In Figure 16, the solid symbols represent the original short crack growth rates, and the hollow symbols are calculated according to Eqn. 5. It is clear from Figure 16 that the El Haddad adjustment shifts the short crack data in the desired direction, *i.e.*, closer to the long crack data. Geometrically, this amounts to moving the short crack rate data points to the long crack growth rate. In other words, if the adjustment was a perfect "fix" for the short crack anomaly, then the hollow symbols would coincide perfectly with the long crack curve.
Using the parameters determined in Figure 5 and the geometry factor solution in Figure 6, the rate equation was integrated[6] to obtain the crack growth. As shown in Figure 17, three cases were considered. The black dashed line shows the results without considering the El Haddad correction, which clearly under-predicts the crack growth rate. The blue solid line shows the results from the El Haddad model with $a_0 = 0.05$ mm, calculated from Eqn. 6. It shifts the crack growth closer to the experimental data in the early stages of crack growth, but under-corrected the data. The red dash-dot line was obtained by a trial-and-error process, which corresponds to $a_0 = 0.103$. The difference in the results plotted in Figure 16 suggests that the threshold stress intensity factor used in the calculation may be too low. As indicated by Eqn. 6, a lower threshold results in a lower value of a_0. Given the uncertainty surrounding threshold crack growth rates, and their correct determination by experiment [16], this apparent sensitivity to the threshold value is not particularly desirable. Also, these values of a_0 are of the same order as the initial crack size for the analysis (0.077 mm) which may be of concern.

[6] The integration was performed using a small Fortran program called "CA-Integration" written by W. Hu. Details are at Appendix B.

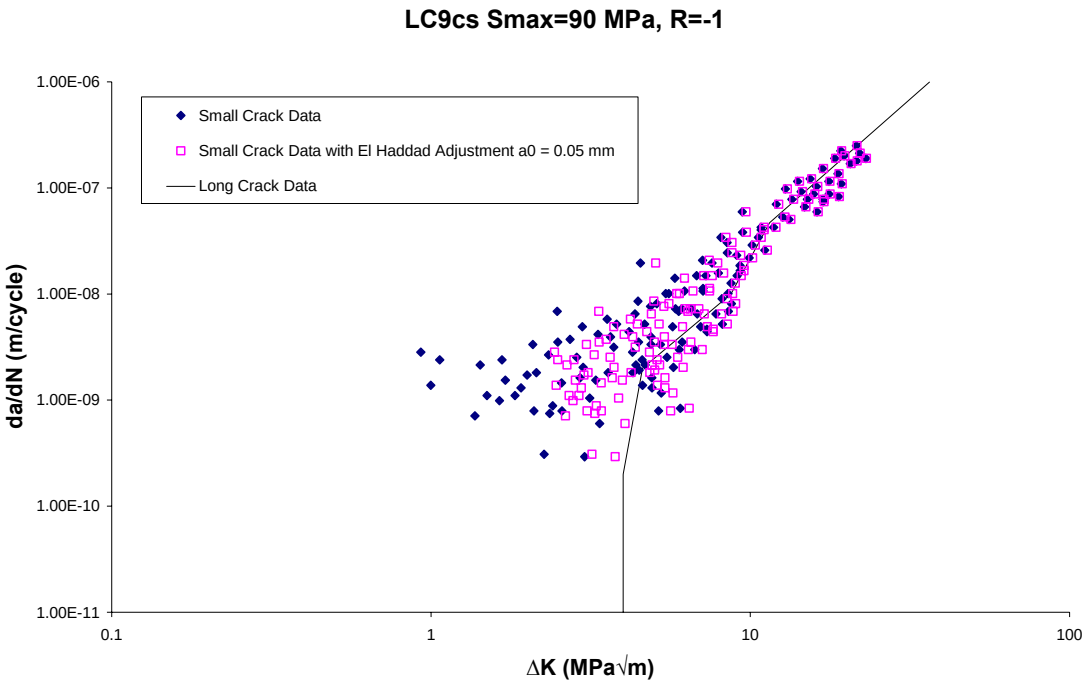

Figure 16 : LC9cs alloy short crack data from [8] subjected to El Haddad adjustment

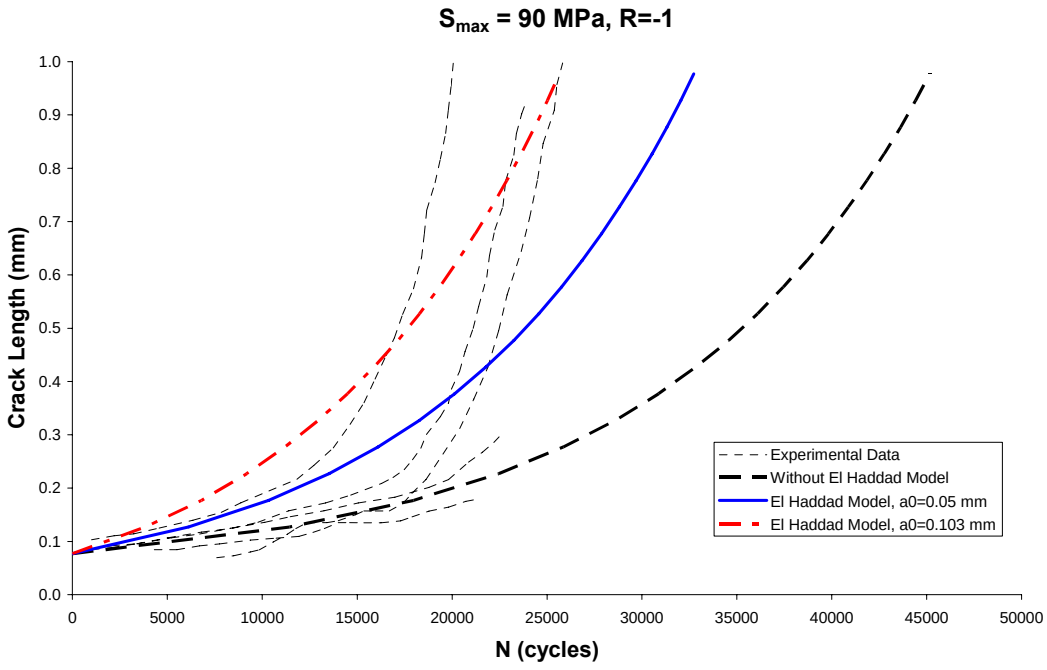

Figure 17: Comparison of crack growth analysis using modified El Haddad approach with experimental data for LC9cs alloy S_{max} = 90 MPa R = -1. Initial crack size = 0.077 mm for all analyses

4.2.2 7075-T6 Alloy

For the 7075-T6 alloy, the values for ΔK_0 and $\Delta\sigma_e$ were available from [8] and they are 2.3 MPa√m and 140 MPa, respectively, which gives $a_0 = 0.0168$ mm according to Eqn. 6. The same analysis for LC9cs was conducted for 7075-T6 alloy using these parameters. Figure 18 plots the crack growth rates according Eqn. 5, with the solid symbols representing the original short crack growth rates and the hollow symbols representing the model results. Again, Figure 18 shows that the El Haddad model shifts the short crack data in the desired direction. Using the parameters determined in Figure 8 and the geometry factor solution in Figure 9, the rate equation was integrated to obtain the crack growth. As shown in Figure 19, three cases were considered. The black dashed line shows the results without considering the El Haddad correction, which clearly under-predicts the crack growth rate. The solid blue line shows the results from the El Haddad model with $a_0 = 0.0168$ mm, calculated from Eqn. 6. It shifts the crack growth closer to the experimental data. The red long dash-short dash line was obtained by a trial-and-error process, which corresponds to $a_0 = 0.02$ mm.

The red long dash-short dash line result is very close to the FASTRAN/CGAP analysis result (see Section 4.3.2 Figure 22). As discussed in [8], the replica technique used to measure the crack lengths was found to have a significant effect on the growth rate. It was found to reduce the growth rate, so as per [8] it is expected that the true behaviour would be closer to the red long dash-short dash curve. Once again, as for the LC9cs material, it appears that the El Haddad model adds too little to the crack length and so the threshold stress intensity may be too low. Similar trends to those observed in the LC9cs case were evident here. In this case the values of a_0 are much larger than the initial crack size for the analysis (0.003 mm) which may be cause for concern.

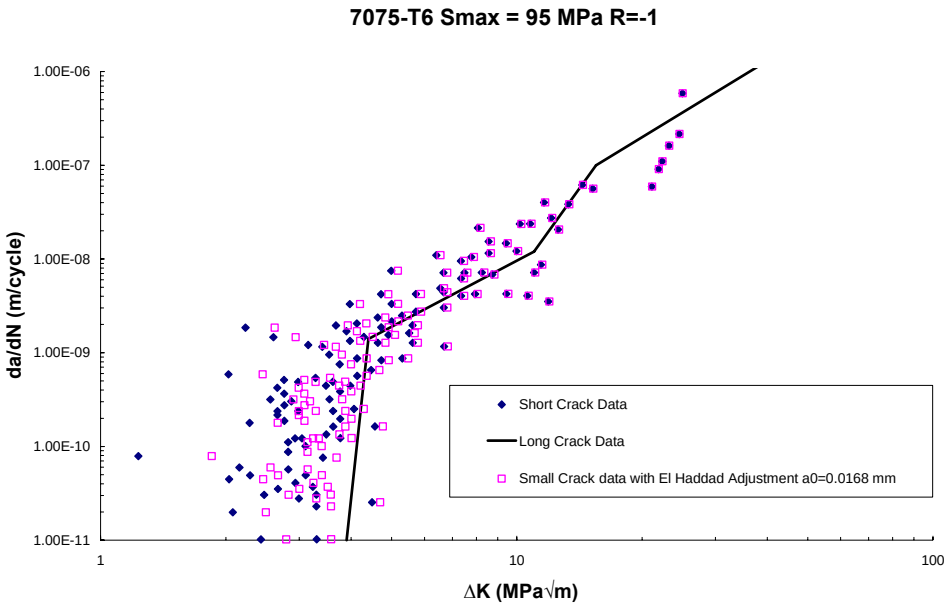

Figure 18: 7075-T6 alloy short crack data from [8] subjected to El Haddad adjustment

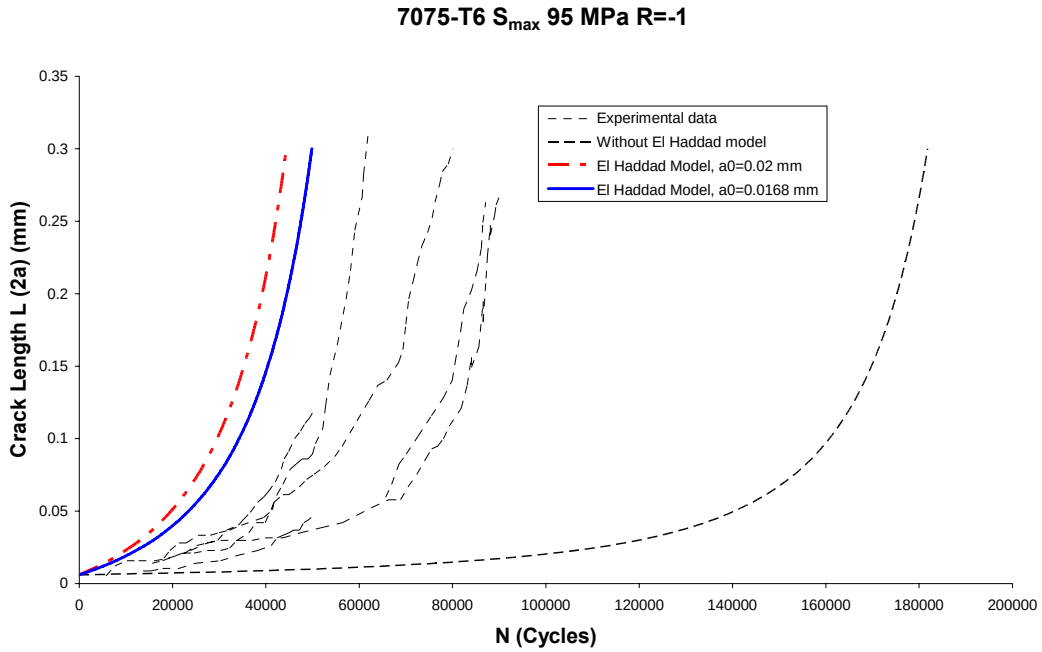

Figure 19: Comparison of crack growth analysis using modified El Haddad approach with experimental data for 7075-T6 alloy Smax 95 MPa case

4.3 FASTRAN Model – Using Long Crack Data to Predict Short Crack Growth

4.3.1 LC9cs Alloy

In [8], the analytical crack closure model employed in FASTRAN [11] was used to model the short crack growth behaviour using crack growth rate data derived from long crack tests. The same model has been employed in a DSTO developed code CGAP and it was used to model the $R = -1$ and $S_{max} = 90$ MPa case. The result is plotted along with the analytical result from [8] in Figure 20. It is evident that the result is very similar to that obtained in [8]. The difference is most likely due to the precision of the numerical values on different computers and compilers used to generate the executable codes[7].

[7] Another possible explanation was discovered later. In e-mail correspondence with the lead author of [8], it became evident that two errors have been made in this report, and they appear to cancel each other out. Firstly, as per [8], in the case of the LC9cs material, a clad correction to the stress intensity solution was implemented in FASTRAN and this was not done in the current work with CGAP. Secondly, there is an error in [8] in that the tabular long crack da/dN vs ΔK_{eff} data as shown in Sections 8.2.1 and 8.2.2 for 7075-T6 and LC9cs respectively are accidentally misplaced (swapped). So, in this report two errors have been made; no clad correction implemented in the stress intensity solution, and effectively using 7075-T6 growth rate data in the LC9cs analysis. As evident in Figure 20, the net effect is that the CGAP analysis conducted here is almost identical to the FASTRAN analysis reported in [8]. It was therefore decided to leave the results as they are. It is considered that the observations of trends and behaviours will still be valid.

CGAP appears to correctly simulate the shape of the crack growth curve, but it under-predicts the crack growth rate when cracks are 0.15 mm or larger.

Figure 21 shows a comparison of the experimental data against the CGAP data obtained by activating both the El Haddad model with $a_0 = 0.103$ mm and the FASTRAN model. This combined model appears to give a much better prediction than either the El Haddad model or the FASTRAN model. More cases need to be studied to assess this combined model.

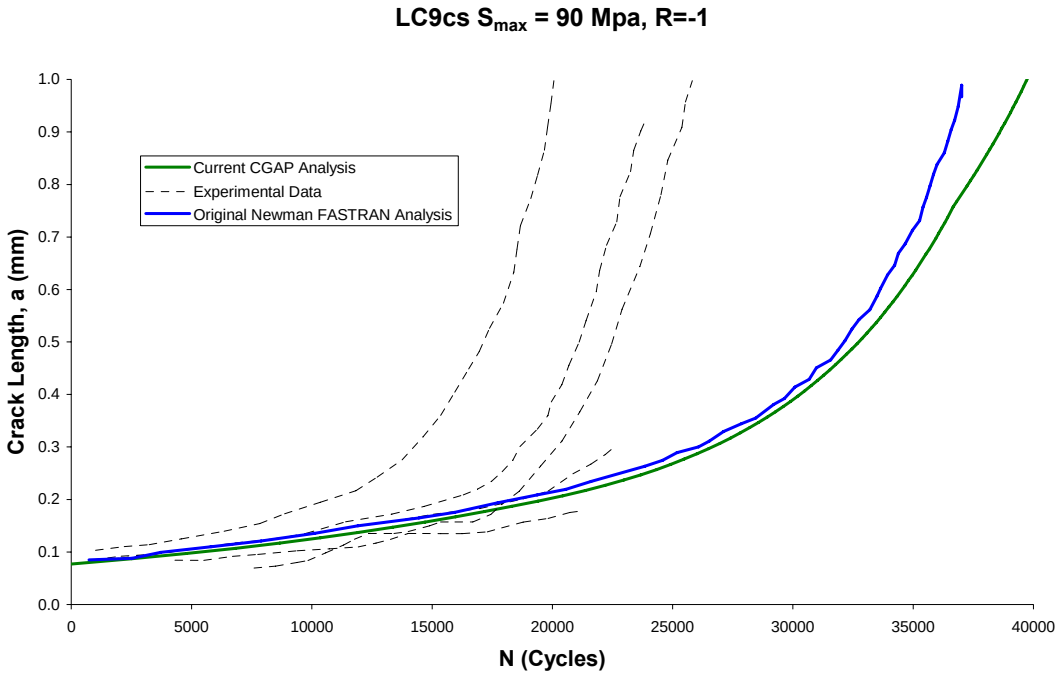

Figure 20: Crack growth comparison, experimental data compared with FASTRAN and FASTRAN/CGAP analyses for LC9cs alloy S_{max} = 90 MPa R = -1. Initial crack size = 0.077 mm

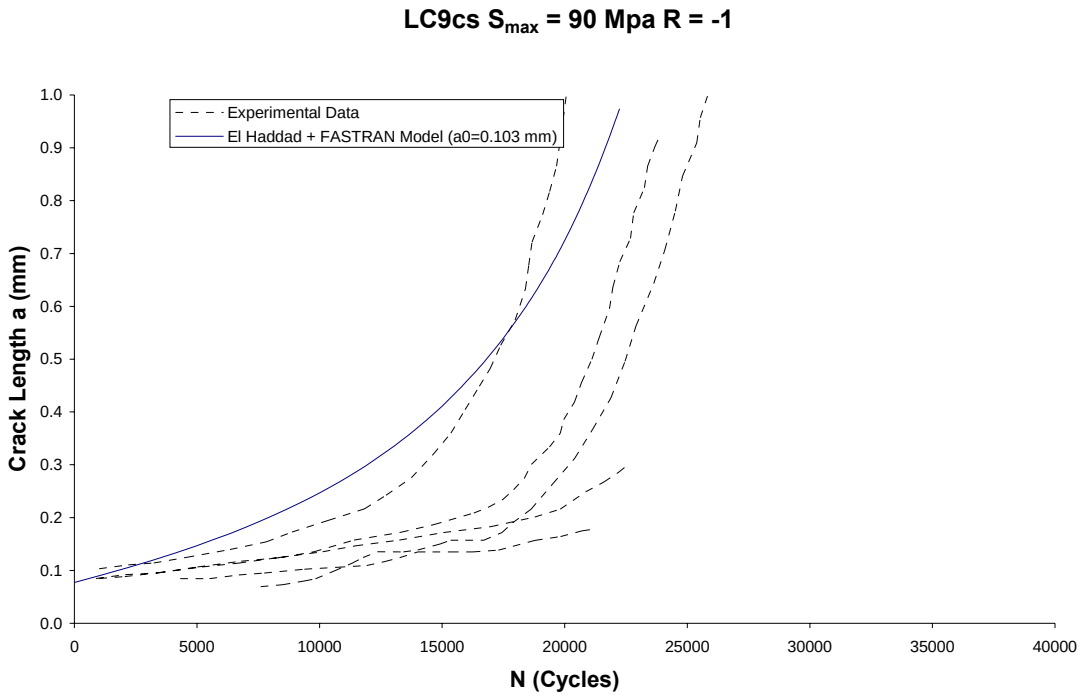

Figure 21: Crack growth comparison, experimental data compared with CGAP results obtained by activating both the FASTRAN model and the El Haddad model with $a_0 = 0.103$ *mm*

4.3.2 7075-T6 Alloy

In [8], the analytical crack closure model employed in FASTRAN [11] was used to model the short crack growth behaviour using crack growth rate data derived from long crack tests. The same code has been employed in a DSTO developed computer program CGAP and it was used to model the $R = -1$ and $S_{\max} = 95$ MPa case. The CGAP results for $R = -1$ and $S_{\max} = 95$ MPa are plotted along with the experimental data from [8] in Figure 22. It is evident that the result is identical to that obtained in [8], and over-predicts the crack growth rate.

As stated earlier, from [8] it is known that the replica technique used to measure crack length, and therefore crack growth rate, affected the growth rate in the 7075-T6 material. However, it had no effect on the LC9cs material, possibly due to the clad layer. The replica technique slowed the rate of crack growth, so the analysis result is possibly closer to where the data would have been without any replica effect.

Figure 23 shows a comparison of the experimental data against the CGAP data obtained by activating both the El Haddad model with $a_0 = 0.086$ mm and the FASTRAN model. In this case the combined model performed worse than the El Haddad model as shown in Figure 19.

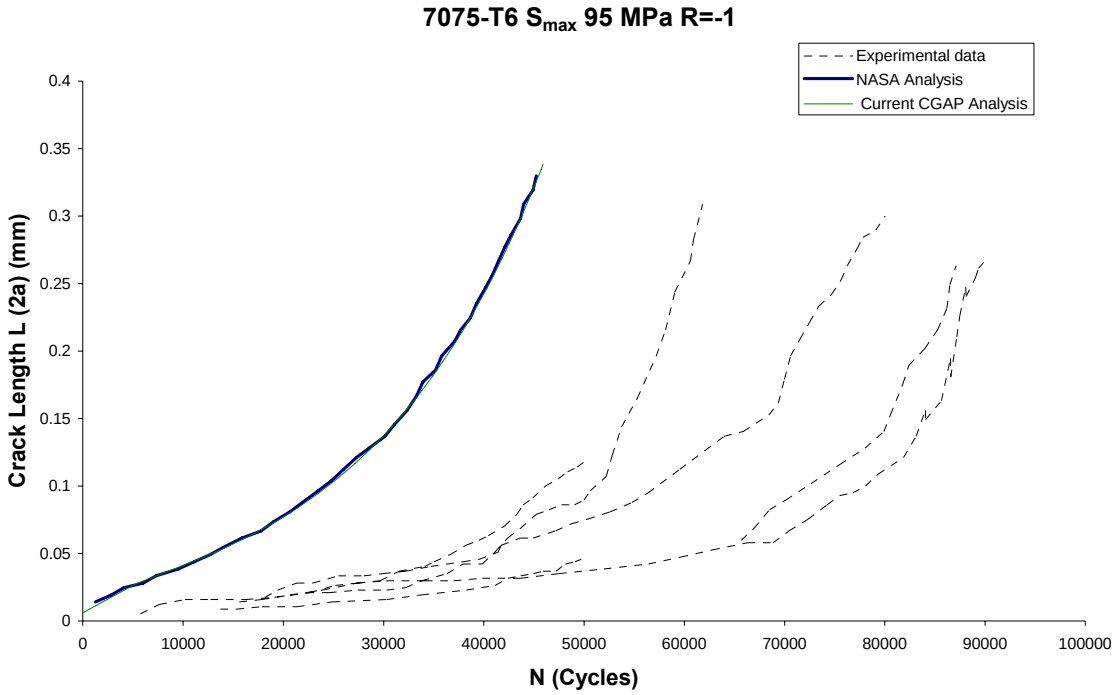

Figure 22: Crack growth comparison, experimental data compared with FASTRAN and FASTRAN/CGAP analyses for 7075-T6 alloy S_{max} = 95 MPa R = -1

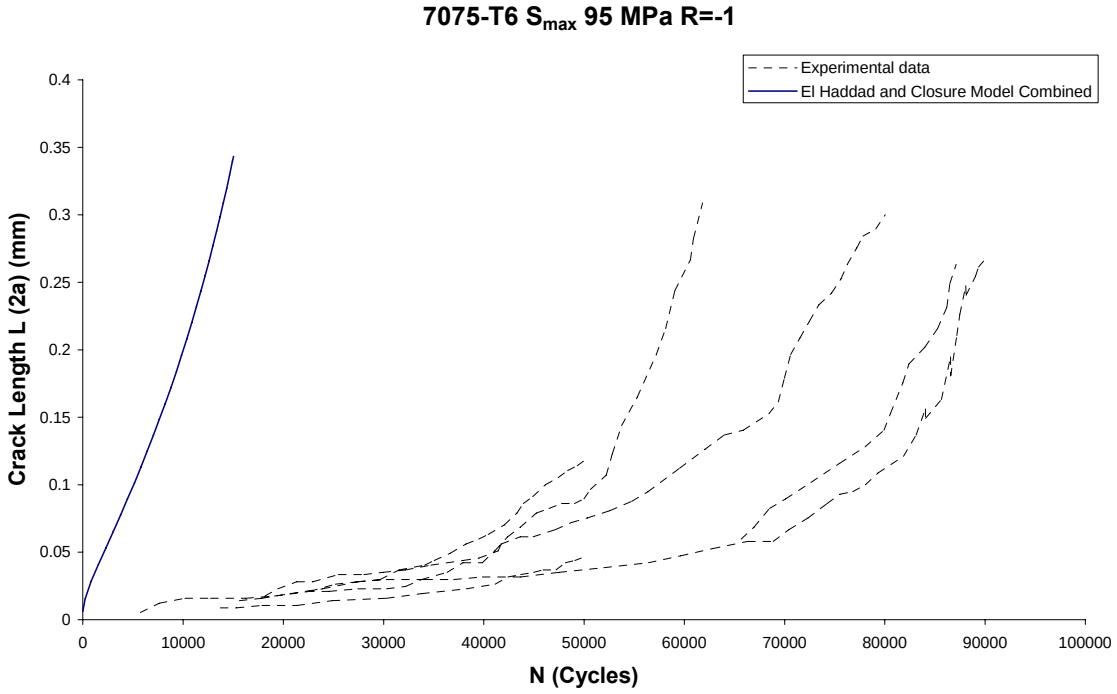

Figure 23: Crack growth comparison, experimental data compared with CGAP results obtained by activating both the FASTRAN model and the El Haddad model with $a_0 = 0.086$ *mm 7075-T6 alloy S_{max} = 95 MPa R = -1*

5. Further Evaluation: Region I and II

This section presents the results of further evaluation of the C^* model, in comparison of the reference models, in predicting short crack growth using long crack growth data, either confined to region I or region I and II, to see whether the C^* model can represent the short and long crack data in a unified manner.

5.1 C* prediction of short crack behaviour using Region I and II long crack data

Figure 16 and Figure 18 plot the long and short crack growth rates for LC9cs and 7075-T6 respectively. The solid lines represent the best fit to the long crack data, and the solid symbols show the short crack data. These figures clearly show that the short and long crack growth rates cannot be uniquely characterised by the SIF Range, a clear demonstration of the breakdown of similitude which occurs for short cracks. Further work was undertaken to determine whether both the long and short crack data can be described in a unified manner under the C^* model. That work is detailed in this section.

In the first instance, it was decided to investigate this situation for both Regions I and II. This was done by determining the value of C^* from the long crack data and undertaking two analyses as follows:

a. Use the long-crack based value of C^* to predict the short crack growth.
b. Compare the long-crack based value of C^* with the value previously determined based on the short crack data.

To do this work as described, an essential ingredient is the crack length associated with the long crack data. Since that information was not known for the LC9cs data, an evaluation was performed using the 7075-T6 data.

The principal author of [8], Dr J. Newman, was able to provide further information about the long crack data for the 7075-T6 material. He provided the stress level used in the tests and details of the geometry of the specimens. The test specimens were finite width and thickness centre crack panels. With this information, it was possible to accurately determine the crack length associated with each pair of crack growth rate and stress intensity range data. It was then also possible to plot crack growth rate against $\frac{\Delta K^3}{\sqrt{a}}$ and fit a straight line through the data as before to determine the value of C^*.

The long crack data as reported in [8] came from two sources; Hudson and Phillips[8] (Figure 24). The Phillips data was from the low to mid portion of the crack growth rata curve, and the Hudson data was from the mid to upper section. The data were processed and plotted to

[8] In an e-mail from Dr J.C. Newman, we were advised that the data cam from work performed by two researchers, "Hudson" and "Phillips" and the data have been identified accordingly

determine C^*. The Phillips result is shown in Figure 25, and the Hudson result in Figure 26. The Hudson data produced such large values of dc/dN and $\Delta K^3/\sqrt{a}$ that it was difficult to distinguish the short crack data on the same plot. A "zoomed in" plot was constructed to show the comparison and it is shown at Figure 27. Another "zoomed in" plot showing both the Hudson and Phillips data is shown at Figure 28.

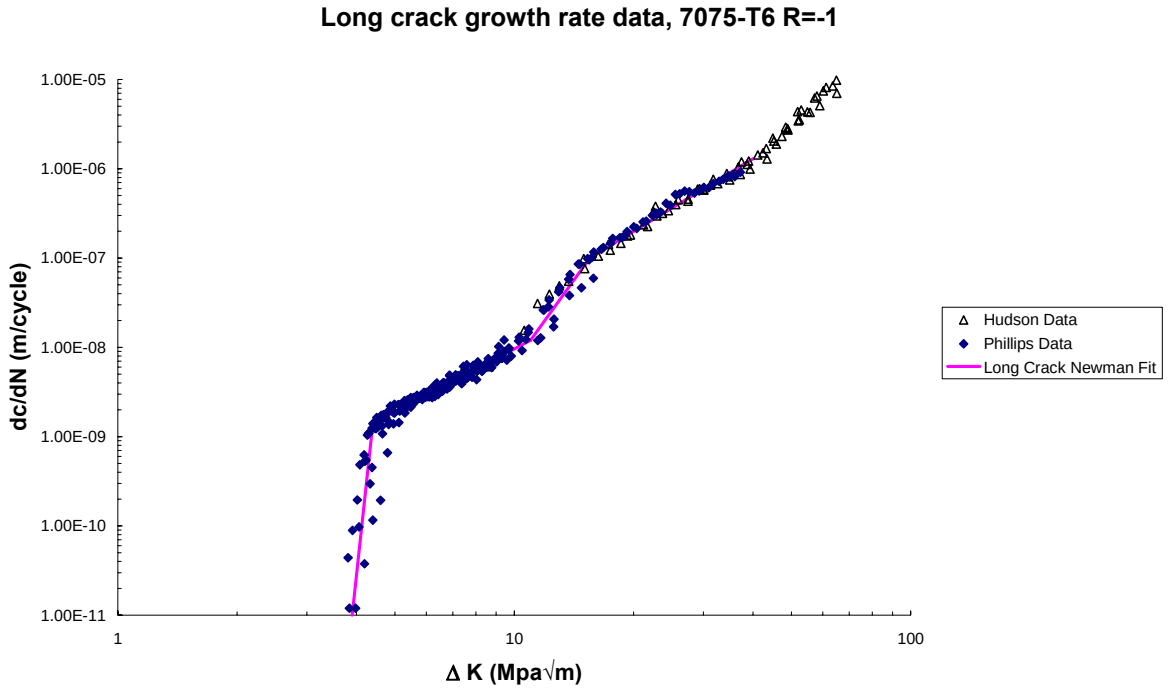

Figure 24: Long crack growth rate data 7075-T6 from [8]

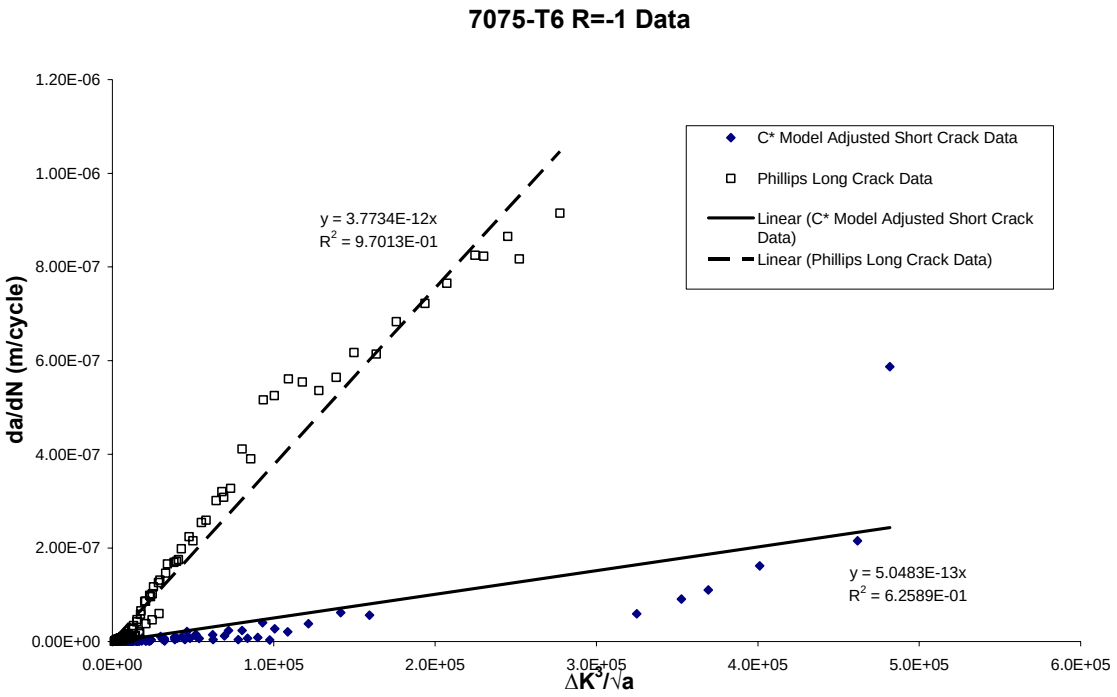

Figure 25: Short crack growth rate and long crack (Phillips) data 7075-T6 alloy R=-1, from [8], replotted according to Eqn. 2

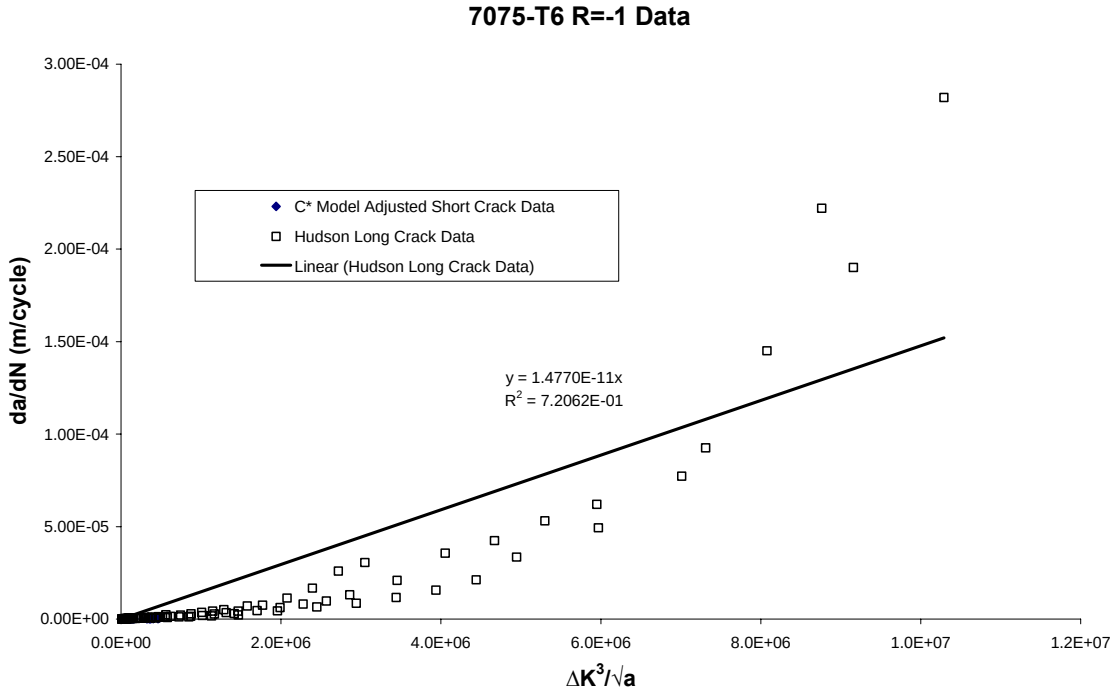

Figure 26: Short crack growth rate and long crack (Hudson) data 7075-T6 alloy R=-1, from[8], replotted according to Eqn. 2

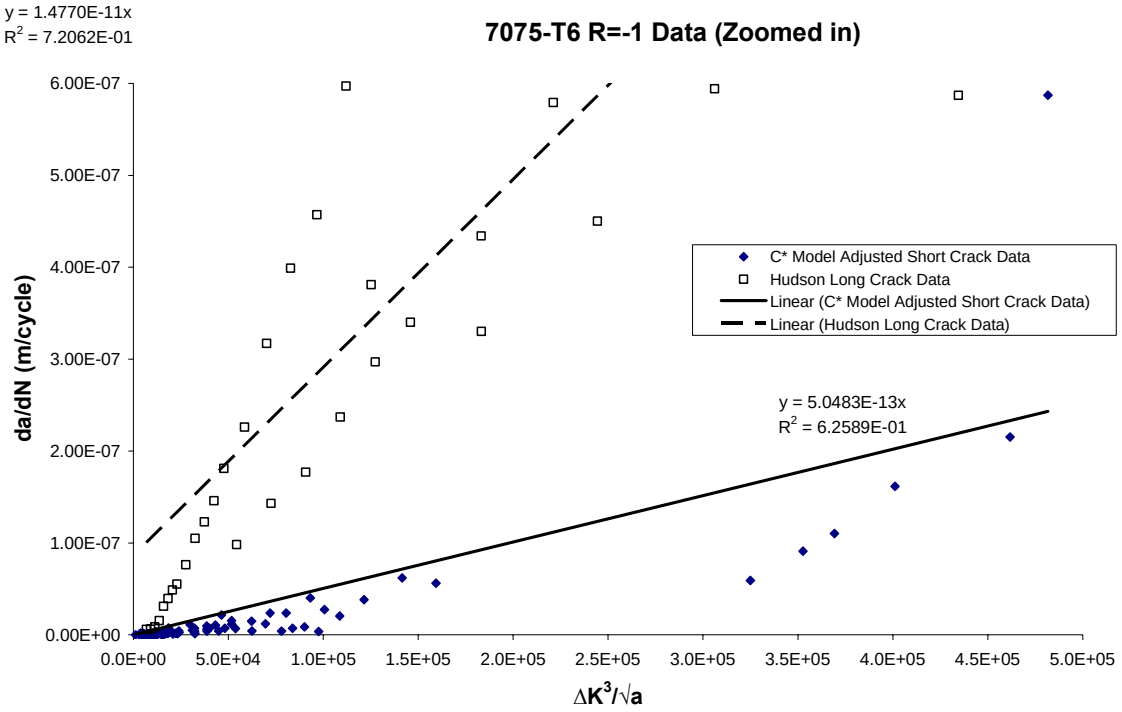

Figure 27: Short crack growth rate and long crack (Hudson) data 7075-T6 alloy R=-1, from[8], replotted according to Eqn. 2 (zoomed in to the short crack data range)

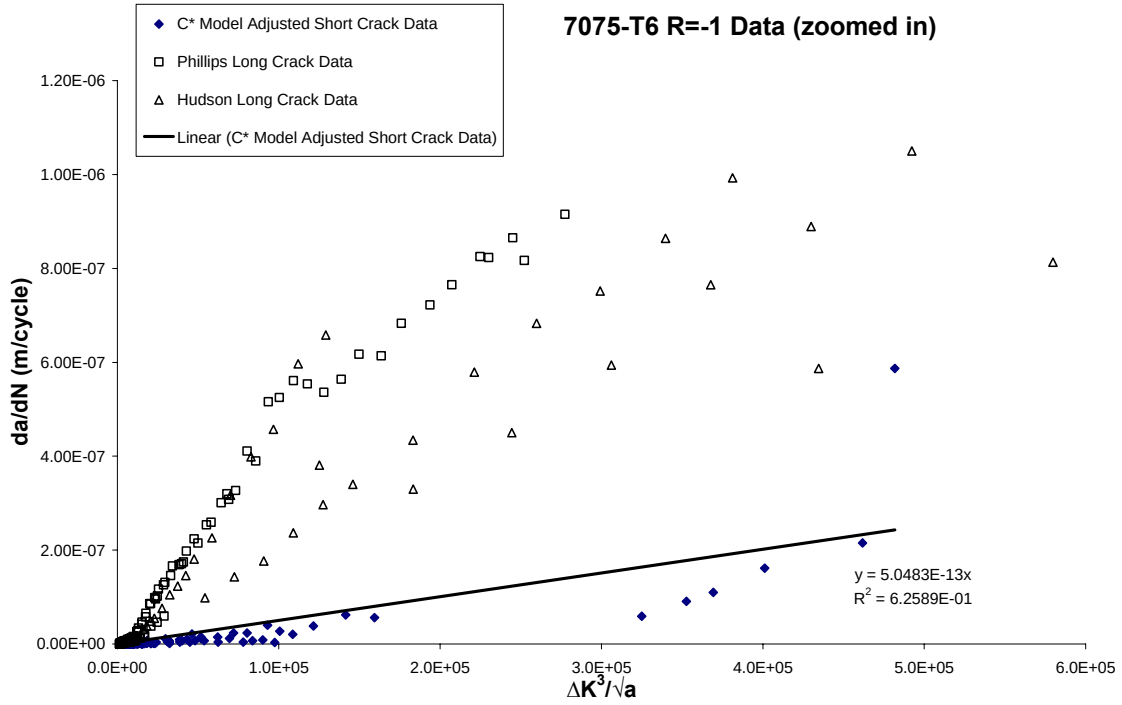

Figure 28: Short crack growth rate and long crack (Hudson and Phillips) data 7075-T6 alloy R=-1, from[8], replotted according to Eqn. 2 (zoomed in to the short crack data range)

A crack growth analysis was then performed using the values of C^* obtained from the Hudson and Phillips data for Regions I and II. This was done in the same manner as earlier in Section 4.1 where it was done using the values of C^* obtained from the short crack data. The results are detailed in Figure 29. It is clear that the prediction using a C^* based on long crack data from Regions I and II produced a very poor correlation in terms of crack growth compared with the short crack data, and also compared with a C^* analysis based on short crack data. The long crack data produced much higher values of C^* which resulted in more rapid crack growth and a significantly shorter predicted life than observed experimentally.

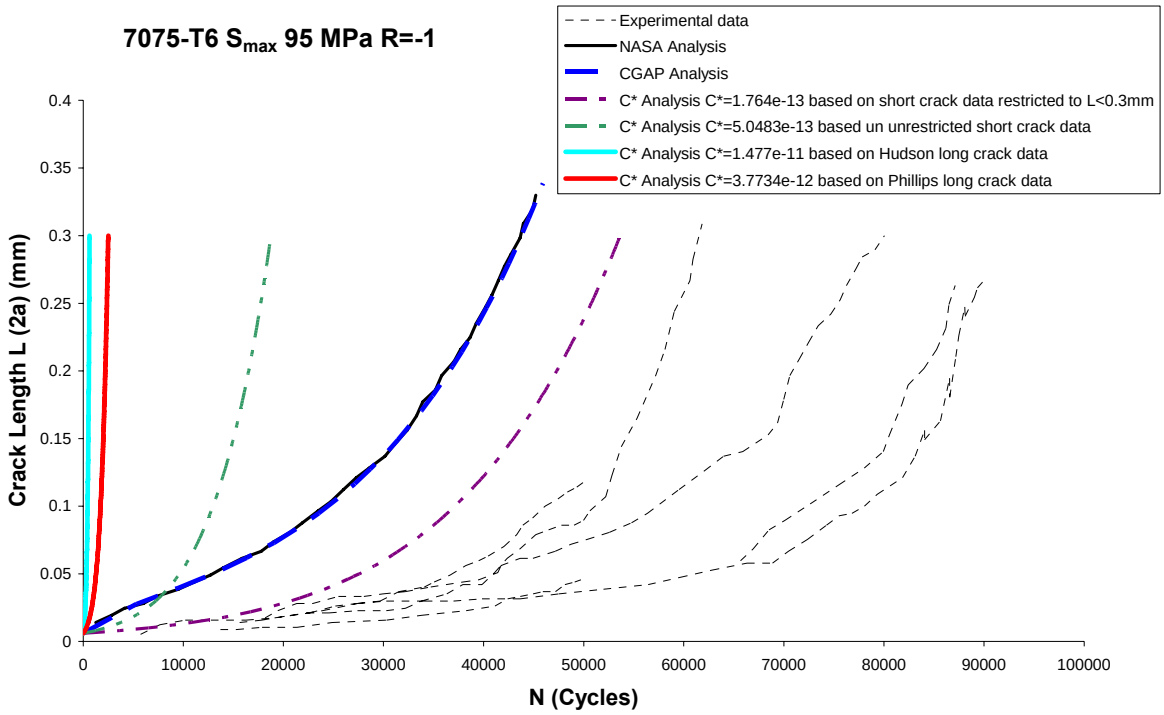

Figure 29: Crack growth curve showing short and long crack (Regions I and II) based C predictions for 7075-T6 alloy*

In terms of the actual values of C^*, a comparison is shown in Table 1. It is clear that values of C^* are orders of magnitude larger when based on the long crack data, and this results in the significantly more rapid crack growth evident in Figure 29.

Table 1: Values of C for 7075-T6 R=-1*

Data source to determine C*	Value of C* (MPa√m, m units)
Unrestricted short crack data	5.0483e-13
Short crack data restricted to L=2a below 0.3 mm	1.764e-13
Hudson data, Region II	1.477e-11
Phillips data, Regions I and II	3.7734e-12

5.2 C* prediction of short crack behaviour using Region I data only

In accordance with the objectives set out for this work (See Section 1) the ability of the C^* model to deal with Region I only was further investigated. Recall that the authors of [5, 6] have claimed that the breakdown of similitude occurs in Region I, and the C^* model offers a resolution of that issue, specifically for Region I.

Again, the crack length associated with the long crack growth rate data is required. This information was known for the 7075-T6 material, thus the data for analysis was for the 7075-T6 material only. The long crack data is plotted in Figure 30, and the portion which would be considered to be "Region I" is clearly evident. A growth rate of 1×10^{-9} m/cycle was identified as the limit of Region I, and that means that in terms of the background data, only a portion of the "Phillips" data is relevant (i.e. none of the "Hudson" data is from Region I).

As before, the data were processed to determine the value of C^*, and the results are shown in Figure 31. Even though significant scatter is evident, it is clear from Figure 31 that the short and long crack data lay in separate distinct regions. Straight line fits were established for these data, although significant scatter was evident. The R^2 values for the linear regression were poor; 0.120 for the Phillips long crack Region I data, and 0.260 for the short crack Region I data. Despite these poor fits, the crack growth analysis using the values of C^* obtained was nevertheless performed. The results are shown in Figure 32. The result for the C^* model based on the long crack Region I data compared well with the experimental short crack data and the CGAP/FASTRAN analyses, which is encouraging. However, it is clear that the result based on the short crack data from Region I was considerably different, and resulted in a six times longer life. This inconsistency does not support the hypothesis that the C^* model resolves the issue of breakdown in similitude for Region I fatigue crack growth. It is important to note that considerable scatter is evident in the Region I data. This scatter is itself evidence of a breakdown of similitude. Whatever the cause of this breakdown, the developers of the C^* model have implied [6] that their model resolves it.

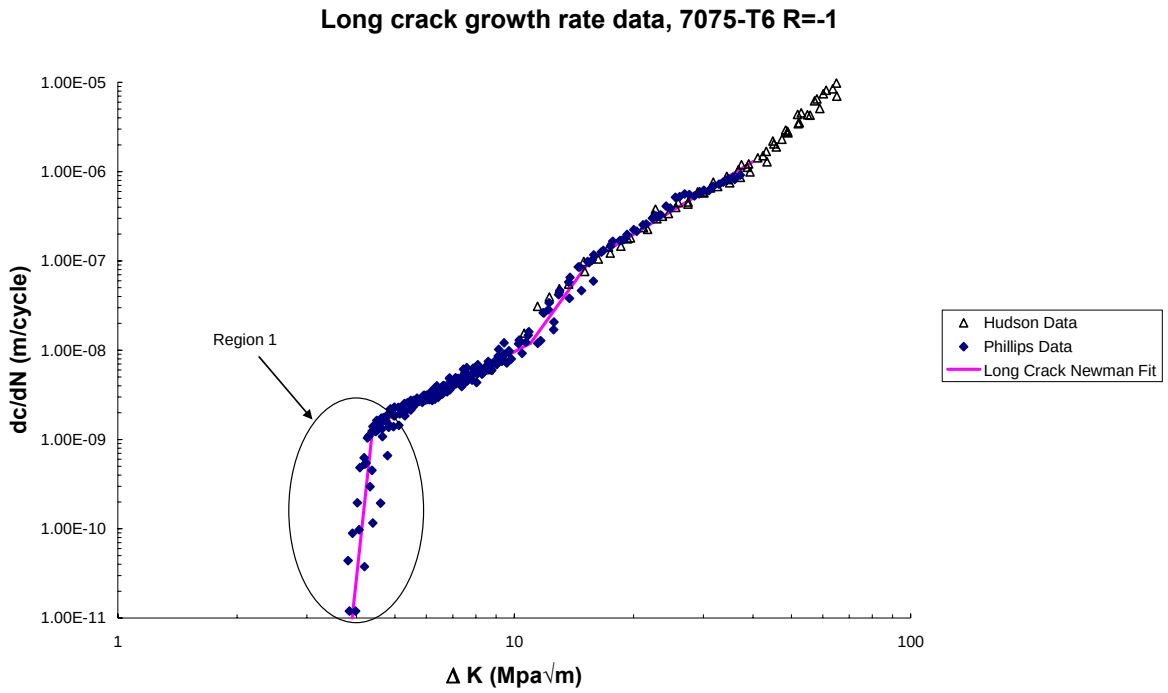

Figure 30: Long crack growth rate data for 7075-T6 material

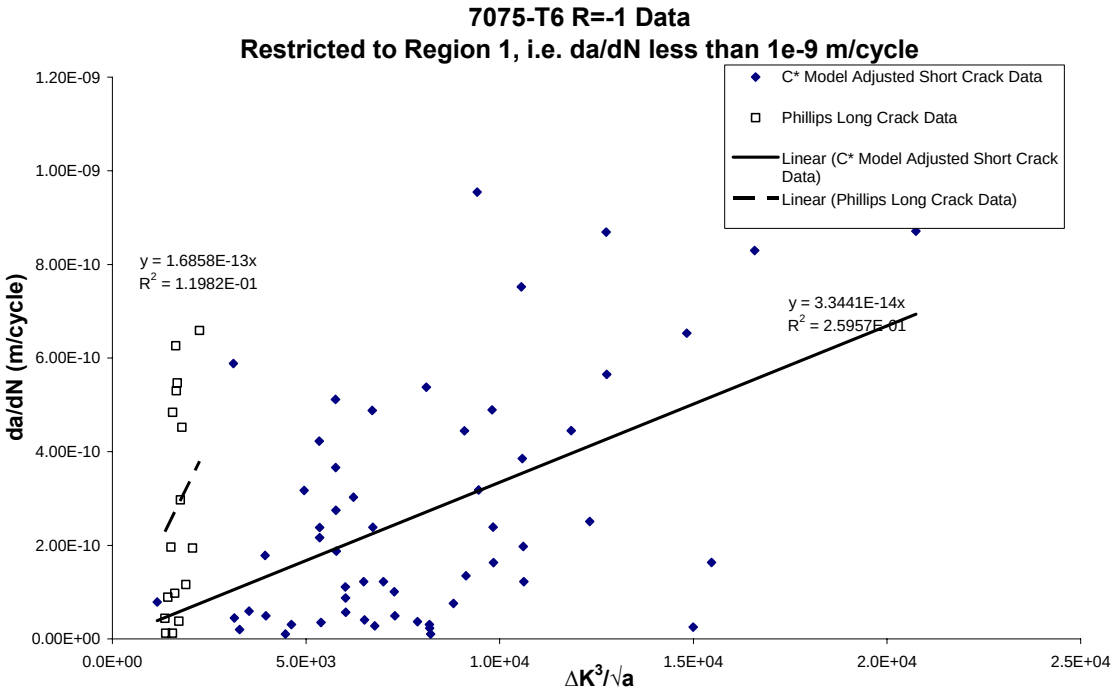

Figure 31: Short crack growth rate and long crack (Phillips) data 7075-T6 alloy R=-1, from [8], for Region I only replotted according to Eqn. 2

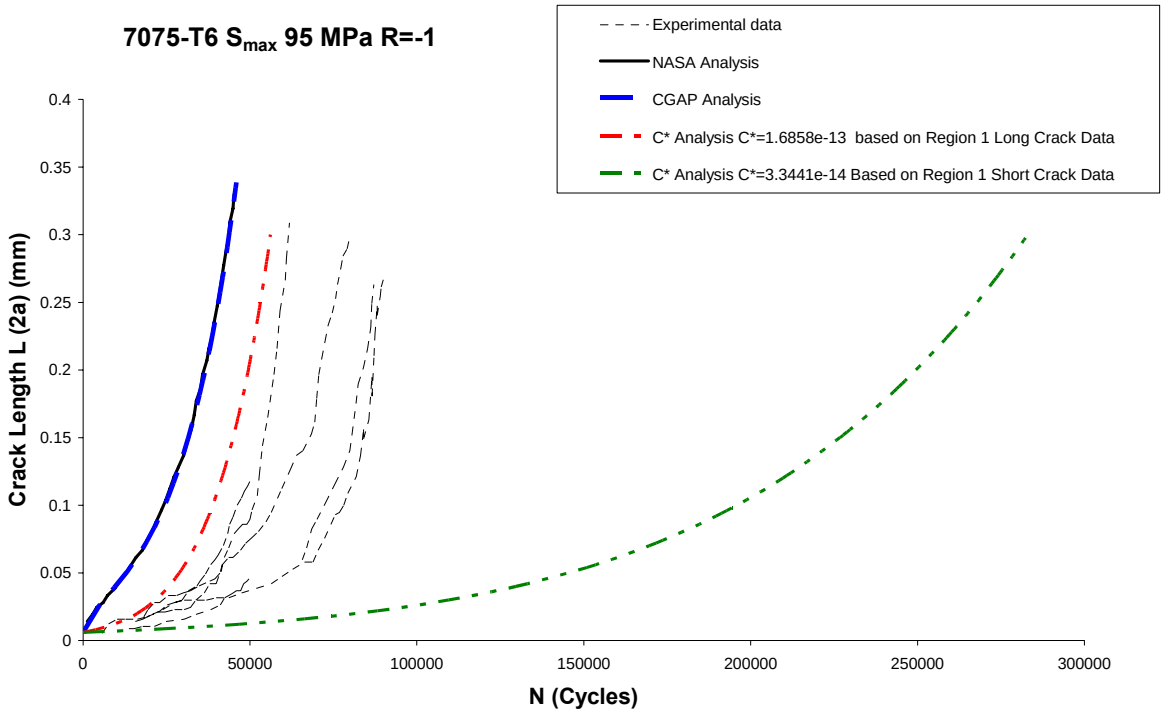

Figure 32: C based crack growth analysis results using long and short crack data restricted to Region I compared with the experimental crack growth data*

The C^* model was thoroughly investigated here for a case where good data for both long and short cracks in Regions I and II were available. The model was able to self-correlate reasonably well when short crack data is used to determine the model parameter (C^*), which is then used to perform an analysis, the results of which are then compared with the original short crack data used to determine C^*. However, in terms of resolving the problem of a breakdown in similitude, the model proved to be ineffective. The inability of the C^* model to resolve the problem of breakdown in similitude was found to occur regardless of whether the data was confined to Region I only, or was from both Regions I and II.

5.3 Further Evaluation of the El Haddad Model

The El Haddad model is conceptually simple. The stress intensity range is increased significantly when the crack length is comparable to a_0, hence raising the crack growth rate, but the effect diminishes when the physical crack becomes large compared to a_0. As demonstrated in Figure 16 and Figure 18, the model appears to account reasonably well for the difference between the long and short crack growth rates for the LC9cs and 7075-T6 materials respectively at R=-1. When this is carried through into a crack growth analysis, the final lives are reasonable, but the shape of the curve is not correct (see Figure 17 and Figure 19 for LC9cs and 7075-T6 respectively). The prediction is improved when the value of a_0 is adjusted to match the experimentally-observed crack growth. The model seems to over predict the growth rate at short crack lengths (around 0.077 mm for the LC9cs and 0.003 mm for the 7075-T6) and under predict the rate when the crack gets larger.

To investigate the effectiveness of the El Haddad model for different stress ratios, the cases of $R = 0, S_{max} = 115$ MPa and $R = 0.5, S_{max} = 185$ MPa for the LC9cs material were also analysed using AFGROW [15], by adjusting the user-defined geometry factor table and the crack length according to Eqn. 5. The crack growth rates for all three stress ratios (-1, 0 and 0.5) are shown in Figure 33 to Figure 35. The investigation showed some interesting results. The model appears to predict a more pronounced short crack effect than is evident in the experimental data. As stated earlier, qualitatively the model seems to achieve the desired effect, that is at larger crack sizes and faster rates the predicted behaviour merges with the long crack data. Unfortunately the crack growth curves for R=0 and R=0.5 cases were not provided in [8], so direct comparisons of the analytical versus experimental crack growth curves could not be made. The data has been requested from the lead author of [8], Dr J. Newman, and if he is able to provide it then such a comparison would be particularly valuable.

Observations on the results are as follows: (1) where available, the data without any adjustment matches the long crack data as expected; (2) the adjustment for the $R = -1, S_{max} = 90$ MPa case shifts the data closer to the short crack data as required (see Figure 33); (3) for the higher stress ratios, the model seems to predict a more pronounced short crack effect than is evident in the experimental data; (4) a point in favour of the model is that the short crack effect is predicted to diminish as ΔK increases such that it approaches the long crack data.

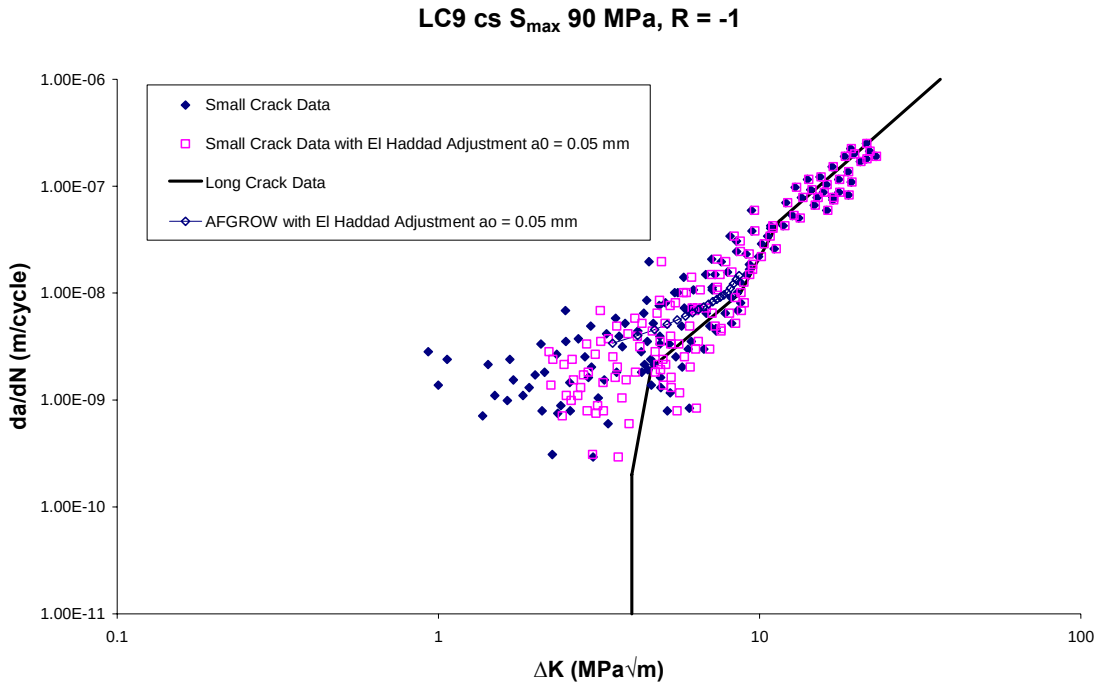

Figure 33: AFGROW model of El Haddad adjustment of ΔK compared with experimental data for LC9cs alloy R = -1 S_{max} = 90 MPa case

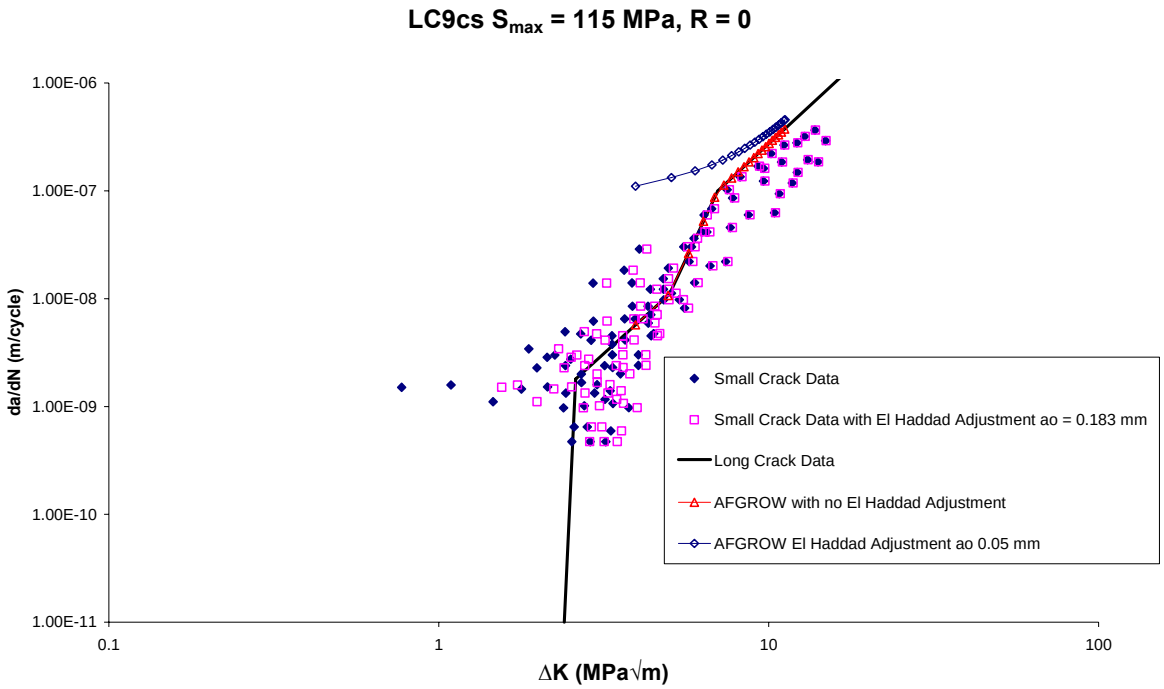

Figure 34: AFGROW model of El Haddad adjustment of ΔK compared with experimental data for LC9cs alloy R = 0 S_{max} = 115 MPa case

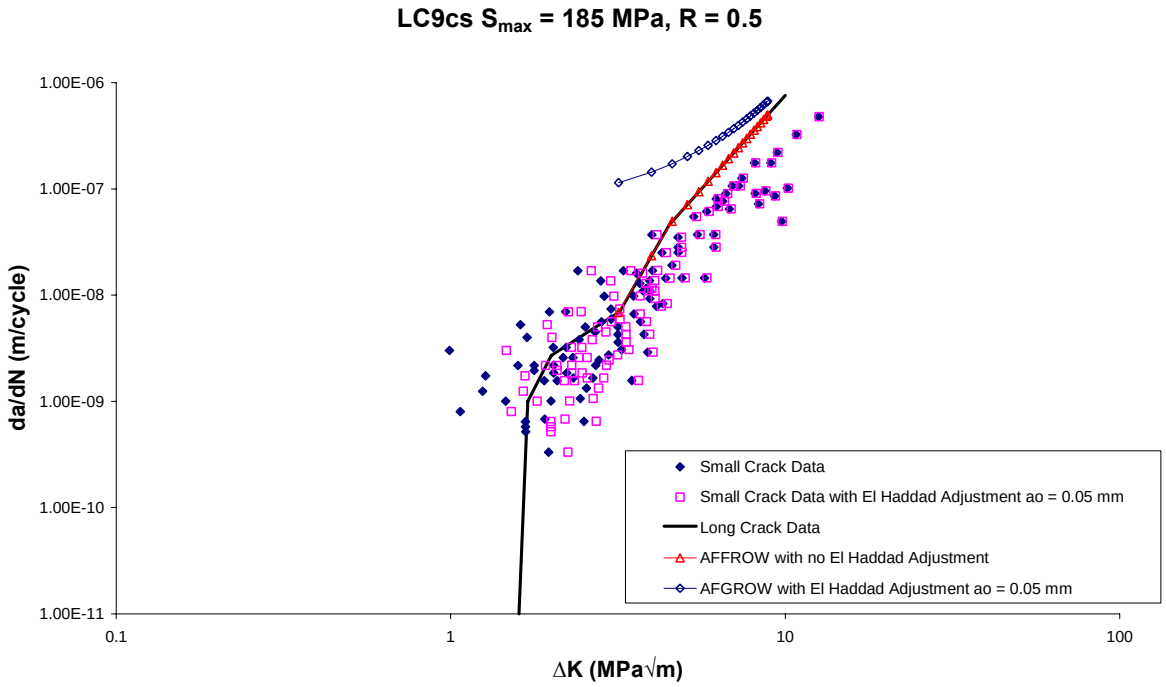

Figure 35: AFGROW model of El Haddad adjustment of ΔK compared with experimental data for LC9cs alloy R = 0.5 S_{max} = 185 MPa case

5.4 Further Evaluation of the FASTRAN Model

The FASTRAN model is based on Irwin's observation that the crack tip plasticity makes the crack behave as if it were slightly longer [17]. Irwin's original idea was to add the whole crack tip plastic zone size ρ to the physical crack length a, but Newman's work [8] has suggested that this may not always give the best prediction. FASTRAN3.8 implements several variants, and numerical results from the current studies and [8] show that the approach can address the short crack effects for a range of constant amplitude and spectrum loading conditions for high strength aluminium alloys. However, the accuracy of the prediction could still be improved, as shown by the comparison in Figure 20 where the model appears to produce significantly longer life than the experiments. It should be noted here that where this is discussed in [8], the authors claim that, based on the growth rates the cracks were exhibiting when the tests were stopped, some of the individual cracks in the experiments *may* have correlated more closely with the analysis had they been allowed to continue their growth. In addition to the modification to the crack length, the crack closure concept inherent in FASTRAN/CGAP also contributes to the improvement in the short crack regime through the variation in the crack opening stress. At the beginning of crack growth, there is no residual plastic deformation on the crack wake, hence the crack opening stress is lower which translates to a higher effective stress intensity range and crack growth rate. As crack front moves forward, residual plastic deformation starts to build up on the crack wake, thus leading to higher crack opening stresses and reduced crack growth rate.

As shown in Figure 21, the combined El Haddad and FASTRAN/CGAP model resulted in an improved solution for the LC9cs case. In the 7075-T6 case, the FASTRAN/CGAP analysis produced more conservative (faster growth) results than the experimental data, but as discussed in [8], this was expected because of the effect that the replica technique had on crack growth. The combined El Haddad and FASTRAN/CGAP analysis (Figure 23) produced more rapid crack growth and a shorter life as expected. The combined El Haddad and FASTRAN/CGAP model produced a better shaped curve than the El Haddad model alone.

6. Discussion

Although great efforts and resources have been spent on the research of short crack growth since Pearson's observation in 1975 [3], and a great deal of qualitative understanding has accumulated as a result, the modelling of short fatigue crack growth is still in an unsatisfactory state. While the blind prediction of long crack growth, supported by numerical calibration, has become a more acceptable tool for the management of aircraft structural integrity, the same cannot be said for short crack growth. Within the framework of LEFM, the objective has been to use experimentally acquired long crack growth data to model the growth behaviour of short cracks, since it is expensive to acquire short crack growth data, and even then it is fraught with inaccuracies. From the viewpoint of material science however, these models are necessarily approximations only. The C^* model is a new idea for dealing with the problem, and it has been evaluated against two other models. The common feature to all three models is that they are readily applicable to real structures subjected to spectrum loading.

With the advancement in quantitative fractography for fracture surfaces [18], there are activities within DSTO to re-examine the classical models and explore new approaches to fatigue crack growth modelling including short cracks. The C^* model examined here is one such example. As quantitative fractography makes the acquisition of crack growth data much easier and less expensive, the new approaches explored so far tend to be phenomenological, including the extension of the Frost-Dugdale log-linear model to spectrum loading, the effective block approach [13], and the C^* model [5-7], although mechanistic modelling is also being pursued, *e.g.*, [19]. As a phenomenological model, the C^* model showed reasonable correlation on the case used to develop the model, but it relies on the availability of short crack growth rate data. *The apparent inability of the model to deal with short and long crack data in a unified manner brings into question its claimed ability to resolve the matter of breakdown of similitude.* Further work is thus needed in order to achieve this objective.

The C^* model as proposed in [5, 6] aims to model the breakdown of similitude in "Region I", as depicted in Figure 1, in crack growth behaviour, although the authors of this report do not agree with the authors of [5, 6] that they have demonstrated a breakdown of similitude, or that they have developed a robust model to deal with it. The authors of [5, 6] assert that because the C^* approach models crack growth rate da/dN as a function of the stress intensity range ΔK, the maximum stress intensity $K_{\max}$, and crack length a, so it is therefore proven that the crack growth rate cannot be a function of ΔK and $K_{\max}$ alone, and this constitutes a proof that similitude does not hold. This assertion of non-similitude is not clearly demonstrated by the data provided in [5, 6]. For instance, it was not demonstrated, using experimental data, that two long cracks of different lengths subjected to the same ΔK and $K_{\max}$ will grow at different rates (as is clearly the case for the long and short crack data from [8] used in this report and shown in Figure 16 and Figure 18, or as is evident in Figure 2 from [20], or Figure 2 from [21], or Figures 10 and 11 from [16]); that short and long cracks can be described by one consistent relationship; and/or that the same relationship could be used to describe the crack growth rates in Region II. *It is also fair to argue that any apparent successful*

empirical modelling of one form does not necessarily preclude the possibility of an alternate form of empirical modelling. Here, we explored these possibilities by: (1) applying the parameter determined using long crack data to predict short crack growth; and (2) comparing the parameters obtained from short and long crack data. We also examined the ability of the C^* model to resolve the issue for Region I data only, or data from both Regions I and II.

In addition, since the practical calculation of ΔK involves a geometry factor β, which is a function of the crack length a, so the said explicit dependence of crack growth rate on crack length may in fact be incorporated into the geometry factor. In any case, [5, 6] only attempted to demonstrate the validity of Eqn. 2 in describing the crack growth rate in Region I for long cracks. Here we have examined its applicability to; (i) short cracks, and (ii) long cracks in Regions I and II, and found that for the cases examined, the C^* model did not resolve the breakdown of similitude.

7. Concluding Remarks

The El Haddad model is conceptually simple and appears to do a reasonable job of accounting for the short crack effect to some extent. However the simple modification alone does not appear to be sufficient. Also the amount added to the crack length can be significant in comparison to the initial crack size for analysis which raises some concern.

The FASTRAN model performs well. The combined FASTRAN and El Haddad model seems to improve the solution further.

In this report, the C^* model proposed by Jones *et al* [5-7] was evaluated against limited experimental data obtained from the open literature. The results of the evaluation show that;

1. if the C^* model parameters were obtained from short crack data, then it can make a reasonable "prediction" for growth of short cracks under the same conditions, but the quality of prediction was only comparable to that of El Haddad or FASTRAN model, both of which use long crack data;
2. the C^* model was not able to unify the short and long crack growth in Region I for the data considered in this report;
3. the C^* model, in the format discussed here, was not able to unify the crack growth in Region I and Region II for long cracks for the data considered in this report.

In short, it was not possible for the authors to use the C^* parameters determined from long crack data to make a reasonable prediction for short crack growth, nor to use the parameters determined from Region I long crack data to make a reasonable prediction for Region II long crack growth. These observations seriously question the validity and usefulness of the C^* model, both in a theoretical sense and in a practical sense.

The apparent inability of the model to deal with short and long crack data in a unified manner brings into question its ability to resolve the matter of breakdown of similitude. It is important to highlight that these conclusions are drawn based on the limited data set used here.

8. Acknowledgements

The authors wish to thank Dr J. Newman from Mississippi State University for his assistance in interpreting the data in [8], and Mr L. Molent from DSTO and Dr R. Jones from Monash University for their assistance in developing an understanding of the C^* model. Thanks also to Mr Phillip Jackson from DSTO for his advice and suggestions.

9. References

1. Suresh, S. and R.O. Ritchie, *Propagation of short fatigue cracks.* International Metals Reviews, 1984. **29**(6): p. 445-476.
2. Paris, P.C. and F. Erdogan, *A critical analysis of crack propagation laws.* Journal of Basic Engineering. Transactions of ASME, 1963. **85**: p. 528-534.
3. Pearson, S., *Initiation of fatigue cracks in commercial aluminium alloys and the subsequent propagation of very short cracks.* Eng. Fract. Mech., 1975. **7**: p. 235-247.
4. El Haddad, M.H., Smith, K.N., and Topper, T.H., *Fatigue crack propagation of short cracks.* Journal of Engineering Materials and Technology, Trans. ASME, 1979. **101**: p. 42-46.
5. Jones, R., L. Molent, and S. Pitt. *Crack growth of physically small cracks*. in *Proceedings of International Conference on Fatigue Damage of Structural Materials VI*. 2006. Hyannis, USA.
6. Jones, R., L. Molent, and S. Pitt, *Crack growth of physically small cracks.* International Journal of Fatigue, 2007.
7. Molent, L., Jones, R., Barter, S. and Pitt, S., *Recent developments in fatigue crack growth assessment.* International Journal of Fatigue, 2006. **38**(12): p. 1759-1768.
8. Newman, J.C., Wu, X.R., Venneri, S.L., and Li, C.G.,Small-Crack Effects in High-Strength Aluminium Alloys,NASA Reference Publication 1309,May 1994
9. Leis, B.N., et al., *Critical review of the fatigue growth of short cracks.* Engineering Fracture Mechanics, 1986. **23**(5): p. 883-898.
10. El Haddad, M.H., K.N. Smith, and T.H. Topper, *Fatigue crack propagation of short cracks.* Journal of Engineering Materials and Technology, Trans. ASME, 1979. **101**: p. 42-46.
11. Newman, J.C., Jr.,FASTRAN II - A fatigue crack growth structural analysis program,NASA TM-104159,1992
12. Hussain, K., *Short fatigue crack behaviour and analytical models: A review analytical models: A review.* Engineering Fracture Mechanics, 1997. **58**(4): p. 327-354.
13. McDonald, M., Molent, L., and Green, A.J.,Assessment of Fatigue Crack Growth Prediction Models for F/A-18 Representative Spectra and Material,DSTO-RR-0312,April 2006
14. Hu, W. and K.F. Walker. *Fatigue Crack Growth from a Notch under Severe Overload and Underload*. in *The International Conference on Structural Integrity and Failure*. 2006. Sydney, Australia.
15. Harter, J.A.,AFGROW user's guide and technical manual,AFRL-VA-WP-TR-2004,
16. Forth, S.C., Newman, J.C., and Forman, R.G., *Evaluation of fatigue crack thresholds using various experimental methods.* Fatigue and Fracture Mechanics, 2002. **33**.
17. Irwin, G.R. *Plastic zone near a crack and fracture toughness*. in *Sagamore Research Conference Proceedings*. 1961.
18. Barter, S.A., *The use of the conventional optical microscope for quantitative fractography*, in *Metallography and mineralogy conference proceedings*. 1991, Institute of metals and materials Australia Limited.
19. White, P., S.A. Barter, and L. Molent, *Observations of crack path changes under simple variable amplitude loading in AA7050-T74561.* International Journal of Fatigue, 2007((to be submitted)).
20. Forth, S.C., Johnston, W.M., and Seshadri, B.R. *The effect of the laboratory specimen on fatigue crack growth rate*. in *Eurpoean Conference on Fracture* 2006.

21. Forth, S.C., James, M.A., Johnston, W.M., and Newman, J.C. *Anomolous fatigue crack growth phenomena in high-strength steel*. in *International Congress on Fracture 11*. 2005. Turin, Italy.

Appendix A: Fortran Program Calc_a

This program solves the following equation:

$$\Delta K = \Delta S \beta(a) \sqrt{\pi a}$$

For a given ΔK and ΔS, knowing the β(a) relationship, a can be calculated numerically.

The input file format is as follows:

ΔS
Number of betas
a_1 $Beta_1$
a_2 $Beta_2$
etc.....
Number of ΔK's
ΔK
ΔK
etc.....

The output file gives two columns being the crack length and ΔK.

The listing of the source code is as follows:

```
!  Calc_a.f90
!
!  FUNCTIONS:
!  Calc_a      - Entry point of console application.
!

!****************************************************************************
****
!
!  PROGRAM: Calc_a
!
!  PURPOSE:  To calculate the crack length from give Dk, DS and beta.
!
!****************************************************************************
****

    program Calc_a
    use nrtype
    implicit none
    integer nbetas, ndks, i
    real(8) beta_a(100), beta(100), ds, dk(1000)
    real(8) a0, bta, get_beta, a, f
    character(80) infile, outfile
    integer blank
    ! Input DS
    ! Input the beta table
```

```
      write(*,*)'Input file format: '
      write(*,*)'delta_s'
      write(*,*)'num_betas'
      write(*,*)'a1 beta1'
      write(*,*)'a2 beta2'
      write(*,*)'...'
      write(*,*)'number_of_dKs'
      write(*,*)'dk1'
      write(*,*)'dk2'
      write(*,*)'...'
      write(*,*)
      write(*,*)'Enter the input file name:'
      read(*,'(A80)') infile

        blank = INDEX (infile, '.', .true.)  ! find the last dot
        if (blank.gt.0) then
              outfile = infile(1:blank) // 'out'
        else  ! there is no extension. Just add '.out'
              outfile = infile(1:len_trim(infile)) // '.out'
        end if

        OPEN(3,FILE=INFILE, STATUS='OLD', err=90001)
        OPEN(4,FILE=OUTFILE, STATUS='REPLACE', err=90002)

      read(3,*) ds
      read(3,*) nbetas
      do i=1,nbetas
          read(3,*) beta_a(i), beta(i)
      end do
      ! Input a list of Dk, and output a list of corresponding a
      read(3,*) ndks
      do i=1,ndks
          read(3,*) dk(i)
      end do

      ! solve the equation F(a)=dk - ds*beta*sqrt(pi*a)= 0, using iterative
  method
      ! starting with a0=0
      a0=0
      do i=1,ndks
          bta=get_beta(beta_a, beta, a0, nbetas)
          a=(dk(i)/ds/bta)**2/pi
          f=dk(i)-ds*bta*sqrt(pi*a0)
          do while(abs(f/dk(i))>0.01)
              a0=a
              bta=get_beta(beta_a, beta, a0, nbetas)
              a=(dk(i)/ds/bta)**2/pi
              f=dk(i)-ds*bta*sqrt(pi*a0)
          end do
          a0=a
          write(4,*) a0, dk(i)
      end do
      90001 continue
      90002 continue
      end program Calc_a

  function get_beta(beta_a, beta, a0, nbetas)
```

```
    ! return the beta value by linear interpolation
    implicit none
    real(8) get_beta
    real(8) beta_a(100), beta(100), a0, locate
    integer loc, left_node, right_node, nbetas
    real(8) l_value, r_value, x_diff
    call locate_x(beta_a, a0, left_node, right_node, nbetas)
      if (left_node .eq. -1) then
          !
          write(4,*) 'An error occurred in elastx(x)'
          write(4,*) 'Analysis terminated.'
          stop
      end if

      if ( left_node .eq. right_node ) then ! we are lucky. it's the
nodal value we need.
            get_beta = beta(left_node)
      else ! interpolation needed. A linear one should do
            l_value = beta(left_node)
            r_value = beta(right_node)
            x_diff = beta_a(right_node) -beta_a(left_node)
            get_beta = l_value + (a0 - beta_a(left_node)) * (r_value -
l_value) / x_diff
      end if
    return
end function get_beta


      subroutine locate_x(nodal_coords, x, l_node, r_node, num_nodes)
      !use bigc, only: exit_code
      ! given x, find the two nodes that contains it
      implicit none
      integer, intent(in) :: num_nodes
      real(8), intent(in) :: x, nodal_coords(100)
      integer, intent(out) :: l_node, r_node
      ! Local variables
      integer inode

      l_node = -1
      r_node = -1
      if(x<nodal_coords(1))then
          l_node=1
          r_node=1
          return
      else if(x>nodal_coords(num_nodes))then
          l_node=num_nodes
          r_node=num_nodes
          return
      end if
      do inode = 1, num_nodes
            if (x .eq. nodal_coords( inode ) ) then
                  l_node = inode
                  r_node = inode
                  exit
            end if
            if (inode .eq. 1) then
```

```
                    if ( x .gt. nodal_coords( 1 ) .and. x .lt.
   nodal_coords( 2 ) ) then
                          l_node = 1
                          r_node = 2
                          exit
                    end if
              else
                    if ( x .ge. nodal_coords( inode -1 ) .and. x .le.
   nodal_coords( inode ) ) then
                          l_node = inode - 1
                          r_node = inode
                          exit
                    end if
              end if
        end do
        if (l_node.eq.0 .or. r_node .eq. 0) then
            write(4,*)
            write(4,*) '***** FATAL ERROR: '
              write(4,*) 'x is not within the range. Program terminates.'
              write(4,*) 'x = ', x
              write(4,*) 'nodal_coords(1) = ', nodal_coords(1)
              write(4,*) 'nodal_coords(num_nodes) = ',
   nodal_coords(num_nodes)
              write(4,*) '***** The first grid coordinate is smaller than
   the radius of the hole.'
              write(4,*)
              l_node = -1
   !          err_code = 91002
        end if
        return
        end subroutine locate_x
```

Appendix B: Fortran Program "CA_Integration"

A source code listing for the program is included below.

The program integrates the following equation:

$$\frac{da}{dN} = Ca^{\phi}\Delta K^{m}$$

Which can be expressed as;

$$N = \int_{N_i}^{N_f} \frac{1}{Ca^{\phi}\Delta K^{m}}\, da$$

Where:

$\Delta K = \Delta\sigma\sqrt{\pi a}\beta$
N is the life in cycles
ΔK is the stress intensity range
Δσ is the applied stress range
β is the geometry factor
C, m and ϕ are constants

The form of the input file (must be named "ds.dat") is as follows:

C m ϕ
Δσ
a_i a_f Δa a_0
Number of betas
a1 beta1
a2 beta2
etc.

Where;

a_i is the initial crack size
a_f is the final crack size
Δa is the crack increment
a_0 is an additional amount to add to the crack length for the El Haddad approach where the stress intensity range solution becomes $\Delta K = \Delta\sigma\sqrt{\pi(a + a_0)}\beta$

The output file is named “fort.2” and the format is three columns of data comprising N (number of cycles), a (crack length) and ΔK

The listing of the source code is as follows:

```
!  CA_Integration.f90
!
!  FUNCTIONS:
!  CA_Integration      - Entry point of console application.
!

!*************************************************************************
****
!
!  PROGRAM: CA_Integration
!
!  PURPOSE:  Integrates the crack growth rate equation for CA loading
!           and user supplied beta-table
!
!*************************************************************************
****
module a_block
    real(8) :: a_beta(100), beta(100), cstar, mstar, phi, a0
    integer :: nbetas
end module a_block

program CA_Integration
    use nrtype
    use a_block
    implicit none
      real(8) ai, af, errabs, errrel, errest, life, ds, ds_const, a,
delta_a, r_func, get_beta
      integer irule, i
    external a_func
    ! Variables
    open(1,file='ds.dat')
    read(1,*) cstar, mstar, phi
    read(1,*) ds
    read(1,*) ai, af, delta_a, a0  ! a0 is the El Haddad parameter
    read(1,*) nbetas
    do i=1,nbetas
        read(1,*) a_beta(i), beta(i)
    end do
    ds_const=cstar*(ds*sqrt(pi)*R_func())**mstar
    ! Body of CA_Integration

      irule = 2
      errabs = 1.D-4
      errrel = 1.D-3
      a=ai

      do while(a<af)
          call DQDAG (a_func, ai, a, ERRABS, ERRREL, IRULE, life, ERREST)
        write(2,*) life/ds_const, a,
ds*get_beta(a_beta,beta,a,nbetas)*sqrt(pi*a)
          a=a+delta_a
    end do
```

```
end program CA_Integration

real(8) function a_func(a)
    use nrtype
    use a_block
    implicit none
    real(8), intent(in):: a
    real(8) bta, get_beta
    bta=get_beta(a_beta, beta, a, nbetas)
    a_func=bta**mstar *(a+a0)**(mstar/2+phi)
    a_func=1/a_func
end function a_func

real(8) function r_func(r)
    implicit none
    real(8),intent(in)::r
    r_func=1
    return
end function r_func

function get_beta(beta_a, beta, a0, nbetas)

    ! return the beta value by linear interpolation
    implicit none
    real(8) get_beta
    real(8) beta_a(100), beta(100), a0, locate
    integer loc, left_node, right_node, nbetas
    real(8) l_value, r_value, x_diff
    call locate_x(beta_a, a0, left_node, right_node, nbetas)
      if (left_node .eq. -1) then
          !
          write(4,*) 'An error occurred in get_beta.'
          write(4,*) 'Analysis terminated.'
          stop
      end if

      if ( left_node .eq. right_node ) then ! we are lucky. it's the
nodal value we need.
            get_beta = beta(left_node)
      else ! interpolation needed. A linear one should do
            l_value = beta(left_node)
            r_value = beta(right_node)
            x_diff = beta_a(right_node) -beta_a(left_node)
            get_beta = l_value + (a0 - beta_a(left_node)) * (r_value -
l_value) / x_diff
      end if
    return
end function get_beta


subroutine locate_x(nodal_coords, x, l_node, r_node, num_nodes)
      !use bigc, only: exit_code
      ! given x, find the two nodes that contains it
      implicit none
      integer, intent(in) :: num_nodes
      real(8), intent(in) :: x, nodal_coords(100)
      integer, intent(out) :: l_node, r_node
```

```
      ! Local variables
      integer inode

      l_node = -1
      r_node = -1
      if(x<nodal_coords(1))then
          l_node=1
          r_node=1
          return
      else if(x>nodal_coords(num_nodes))then
          l_node=num_nodes
          r_node=num_nodes
          return
      end if
      do inode = 1, num_nodes
            if (x .eq. nodal_coords( inode ) ) then
                  l_node = inode
                  r_node = inode
                  exit
            end if
            if (inode .eq. 1) then
                  if ( x .gt. nodal_coords( 1 ) .and. x .lt.
nodal_coords( 2 ) ) then
                        l_node = 1
                        r_node = 2
                        exit
                  end if
            else
                  if ( x .ge. nodal_coords( inode -1 ) .and. x .le.
nodal_coords( inode ) ) then
                        l_node = inode - 1
                        r_node = inode
                        exit
                  end if
            end if
      end do
      if (l_node.eq.0 .or. r_node .eq. 0) then
          write(4,*)
          write(4,*) '***** FATAL ERROR: '
            write(4,*) 'x is not within the range. Program terminates.'
            write(4,*) 'x = ', x
            write(4,*) 'nodal_coords(1) = ', nodal_coords(1)
            write(4,*) 'nodal_coords(num_nodes) = ',
nodal_coords(num_nodes)
            write(4,*) '***** The first grid coordinate is smaller than
the radius of the hole.'
            write(4,*)
            l_node = -1
!           err_code = 91002
      end if
      return
end subroutine locate_x
```

DEFENCE SCIENCE AND TECHNOLOGY ORGANISATION
DOCUMENT CONTROL DATA

1. PRIVACY MARKING/CAVEAT (OF DOCUMENT)

2. TITLE

Evaluation of the C* Model for Addressing Short Fatigue Crack Growth

3. SECURITY CLASSIFICATION (FOR UNCLASSIFIED REPORTS THAT ARE LIMITED RELEASE USE (L) NEXT TO DOCUMENT CLASSIFICATION)

Document	(U)
Title	(U)
Abstract	(U)

4. AUTHOR(S)

K.F. Walker and W. Hu

5. CORPORATE AUTHOR

DSTO Defence Science and Technology Organisation
506 Lorimer St
Fishermans Bend Victoria 3207 Australia

6a. DSTO NUMBER	6b. AR NUMBER	6c. TYPE OF REPORT	7. DOCUMENT DATE
DSTO-TR-2185	AR-014-281	Technical Report	October 2008

8. FILE NUMBER	9. TASK NUMBER	10. TASK SPONSOR	11. NO. OF PAGES	12. NO. OF REFERENCES
2007/1087992/1	AIR 07/051	DGTA	51	21

13. URL on the World Wide Web

http://www.dsto.defence.gov.au/corporate/reports/DSTO-TR-2185.pdf

14. RELEASE AUTHORITY

Chief, Air Vehicles Division

15. SECONDARY RELEASE STATEMENT OF THIS DOCUMENT

Approved for public release

OVERSEAS ENQUIRIES OUTSIDE STATED LIMITATIONS SHOULD BE REFERRED THROUGH DOCUMENT EXCHANGE, PO BOX 1500, EDINBURGH, SA 5111

16. DELIBERATE ANNOUNCEMENT

No Limitations

17. CITATION IN OTHER DOCUMENTS Yes

18. DSTO Research Library Thesaurus

Military aircraft, Fatigue (materials), Mathematical modelling, Airframes, Aircraft structures, Crack propagation, Stress intensity factors

19. ABSTRACT

The C* model has been proposed to account for the breakdown of K-similitude which occurs for short cracks. The model is based on the concept that crack growth rate is dependent not only on the stress intensity factor range, but also on crack length. This report evaluates the C* model using experimental data from the open literature. For comparison, two other models, the El Haddad model and the FASTRAN model, were also evaluated for their capability in dealing with the same problem. The objective of the evaluation was to assess the performance of the C* model compared with the other two models in treating short and long crack growth in a unified manner, and to illustrate their merits and shortcomings. For the cases tested, the C* model was found to be ineffective in resolving the issue of breakdown of similitude for short cracks, and was of less practical use than the other models.